photonics

MDPI

Review

Advances in Optical Fiber Speckle Sensing: A Comprehensive Review

Ivan Chapalo [1,2], Andreas Stylianou [3], Patrice Mégret [1] and Antreas Theodosiou [4,5,*]

[1] Electromagnetism and Telecom Department, University of Mons, 7000 Mons, Belgium; ivan.chapalo@umons.ac.be (I.C.); patrice.megret@umons.ac.be (P.M.)
[2] Foundation for Research and Technology Hellas (FORTH), Institute of Electronic Structure and Laser (IESL), 70013 Heraklion, Greece
[3] School of Sciences, European University Cyprus/EUC Research Centre, 1516 Nicosia, Cyprus; an.stylianou@euc.ac.cy
[4] Photonics Research Center (PRC), Lumoscribe Ltd., 8201 Paphos, Cyprus
[5] Institute of Photonics and Electronics (UFE), The Czech Academy of Sciences, Chaberska 57, 8-Kobylisi, 18200 Prague, Czech Republic
* Correspondence: theodosiou.antreas@lumoscribe.com

Abstract: Optical fiber sensors have been studied, developed, and already used in the industry for more than 50 years due to their multiplexing capabilities, lightweight design, compact form factors, and electromagnetic field immunity. The scientific community continuously studies new materials, schemes, and architectures aiming to improve existing technologies. Navigating through diverse sensor technologies, including interferometry, intensity variation, nonlinear effects, and grating-based sensors, fiber specklegram sensors (FSSs) emerge as promising alternatives due to their simplicity and low cost. This review paper, emphasizing the potential of FSSs, contributes insights to the present state and future prospects for FSSs, providing a holistic view of advancements propelling FSSs to new frontiers of innovation. Subsequent sections explore recent research, technological trends, and emerging applications, contributing to a deeper understanding of the intricacies shaping the future of FFS sensor technologies.

Keywords: optical fiber sensors; optical fibers; interferometric sensors; multimode optical fibers; sensing; image processing; demodulation algorithms; future sensing solutions; fiber specklegram sensors; speckle interferometry

Citation: Chapalo, I.; Stylianou, A.; Mégret, P.; Theodosiou, A. Advances in Optical Fiber Speckle Sensing: A Comprehensive Review. *Photonics* **2024**, *11*, 299. https://doi.org/10.3390/photonics11040299

Received: 2 March 2024
Revised: 20 March 2024
Accepted: 21 March 2024
Published: 26 March 2024

1. Introduction

In the dynamic landscape of sensing technologies, the ubiquity of optical fiber sensors has propelled them to the forefront of scientific and industrial applications. Their widespread use is underpinned by distinctive advantages, such as multiplexing capabilities, lightweight construction, compact form factors, and immunity to electromagnetic fields [1–3]. Optical fiber sensors have become indispensable tools across an array of disciplines, demonstrating their efficacy in medical diagnostics [4,5], structural health monitoring [6–9], robotics [10,11], gait analysis [12], and the detection of chemical compounds [13]. The adaptability and versatility of optical fiber sensors have prompted researchers to explore various technological approaches, each contributing to the ongoing evolution of this field. A plethora of optical fiber sensor technologies have been proposed, capitalizing on distinct effects on optical fibers to achieve specific sensing outcomes. These include interferometry [14], intensity variation [15], nonlinear effects [2,16], grating-based sensors [17], and fiber specklegram sensors (FSSs) as a type of interferometric sensor [18]. The diversity within these approaches underscores the richness of possibilities in optical fiber sensing, allowing for customization to suit the unique requirements of different applications.

The dichotomy between multimode and single-mode optical fibers (SMF) adds another layer of complexity to the sensor landscape. On the one hand, multimode optical fibers (MMFs) are accompanied by drawbacks such as modal dispersion, modal noise, and modal

behavior complexity. On the other hand, MMFs offer practical advantages such as their ease of coupling. Moreover, multimode light propagation allows for increasing information capacity by applying spatial division multiplexing techniques [19] and opens the possibility for mode-related fiber sensing techniques [18]. Conversely, single-mode optical fibers, designed for the propagation of only one mode of light, provide higher fidelity in signal transmission but may be constrained in applications that demand greater modal diversity. Striking a balance between these considerations is crucial in developing optical fiber sensors tailored to specific use cases.

The inherent complexity of optical fiber sensors demands a nuanced understanding of each sensor's approach. For instance, sensors based on fiber nonlinear effects eliminate the need for structural modifications to the fiber, making them suitable for seamless integration into existing optical fiber communication lines [20]. However, the requirement for bulky and expensive equipment for interrogation poses challenges in practical implementation and may limit spatial resolution [21]. Fiber Bragg grating (FBG) sensors, a significant category within optical fiber sensors, provide solutions for quasi-distributed sensing applications but introduce complexities related to both sensor interrogation and the specialized and sometimes expensive equipment needed for grating inscription and interrogation [22–24]. Intensity-variation-based sensors offer a cost-effective alternative, analyzing power variations concerning a specific measurement [25]. Nevertheless, their low sensitivity and susceptibility to light source power variation necessitate additional compensation techniques to maintain accuracy and reliability [26].

In response to the quest for a sensor that amalgamates reliability with key parameters like compactness, lightweight design, simplicity, and cost-effectiveness, FSSs have emerged as a promising alternative in the optical fiber sensing landscape [18,27]. Operating by analyzing the specklegram created on the end facet of a multimode fiber illuminated with a coherent light source, FSSs correlate this speckle pattern with external fiber perturbations (EFPs). Notably, FSSs exhibit potentially multipoint capabilities through the use of beams with different angular separations or wavelengths [28], offering a portable and low-cost interrogation system that stands out in contrast to bulkier and more expensive alternatives.

As technology continues its relentless march forward, the intricate interplay between different types of optical fiber sensors, the challenges associated with their designs, and the continuous innovations in sensing methodologies form the crux of an exciting and dynamic field of research. This review aims to delve deeper into the promising field of FSSs, providing insights into the present state and future prospects of current technology. Through a nuanced examination of the complexities and advancements, this paper seeks to contribute to a deeper understanding of the intricacies that shape the future potential of FSSs. Further sections explore recent research findings, technological trends, and emerging applications, offering a holistic view of the advancements propelling FSSs into prospects with improved sensing capabilities.

2. Brief Historical Background and Terminology

The first research works related to fiber speckles appeared in the 1970s: in 1976, the investigations of speckle patterns at MMF outputs were presented in a number of papers [29,30]. Immediately after, the first works dedicated to acoustic sensors based on intermodal interference were published in 1977–1979 [31–33]. FSSs have been attracting noticeable attention from researchers due to their simplicity and low cost: the basic scheme required just a coherent light source, a multimode fiber, and a photodetector (PD) or CCD/camera matrix (Figure 1a). Moreover, with their interferometric nature, FSSs demonstrated high sensitivity to external fiber perturbations (EFPs); however, it was estimated as 10–1000 times less depending on the number of interfering modes when compared to other interferometric schemes such as two-arm interferometers [32,33]. Along with advantages, FSSs also exhibited several limitations, the main limitations of which were the strong nonlinearity of a transfer function and signal fading. Therefore, a significant number of research works have focused on overcoming these problems (see Section 4), while other papers have

addressed FSS applications (see Section 5). It should be mentioned that in different works, FSSs—sensors based on intermodal interference and analysis of the speckle pattern—are also referred to as mode–mode interferometers [32,34], multimode interferometers [35,36], statistical-mode sensors [37], and intermodal fiber interferometers [38–40].

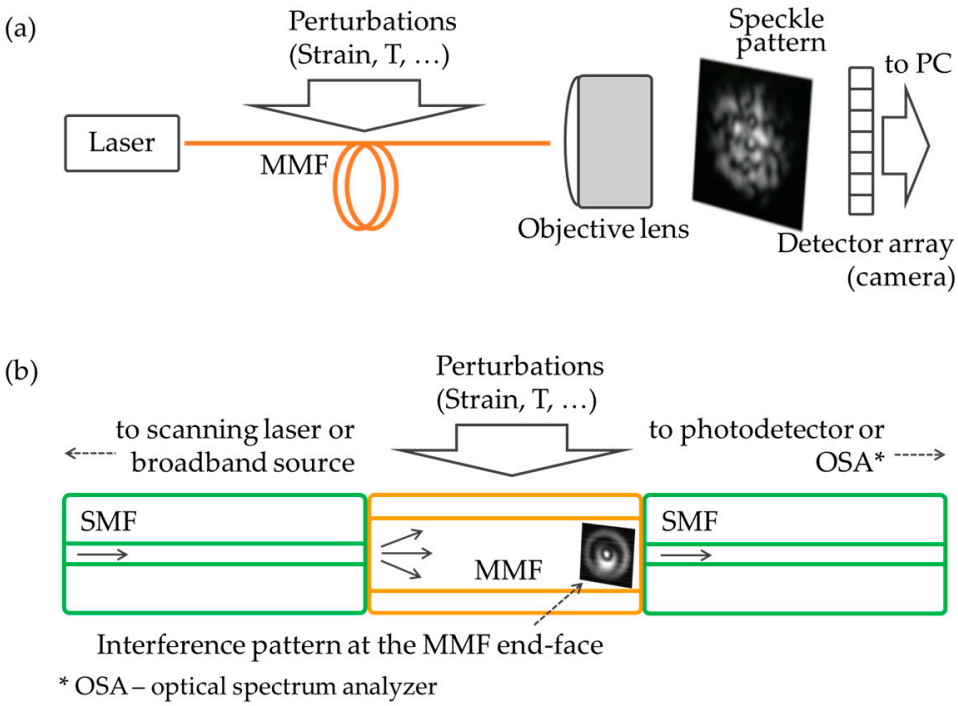

Figure 1. Basic schematic of (**a**) fiber specklegram sensor (intermodal fiber interferometer) and (**b**) interferometric SMS sensor.

In the 2000s, another direction of intermodal interferometric sensors was launched [41]. The basic scheme of a sensor consists of a short piece of MMF coaxially aligned and sandwiched between two SMFs. The input SMF excites a certain number of modes in the MMF. The interferometric pattern formed at the MMF output facet is spatially filtered by the output SMF. Thus, the output signal is proportional to the light intensity "accepted" by the output SMF according to the interference pattern formed at the MMF facet. Unlike "traditional" FSSs, which in the basic configuration utilize a coherent light source with a static wavelength, this type of sensor operates in the spectral domain: either a scanning laser at the input and a PD at the output, either a broadband source at the input and an optical spectrum analyzer (OSA) or a spectrometer at the output have been utilized in this case. Since the interferometric signal is sensitive to both EFPs and laser frequency (wavelength), the output OSA spectrum (or the PD signal formed by a wavelength scan of the scanning laser) represents an interferometric signal of a complex shape, which transforms under external perturbations of the MMF. Thus, tracking a certain interferometric maximum or minimum in a consecutively updating spectrum allows the measurement of EFPs. According to the basic structure of this type of sensor, in the literature, they are usually referred to as single-mode–multimode–single-mode (SMS) sensors (Figure 1b). It should be noted that in SMS sensor designs, the MMF section can be replaced by various specialty fibers providing unique properties and sensitivity to a desired measurand. For example, a standard MMF can serve as a temperature sensor, while a section of a coreless fiber allows for the sensing of refractive index. SMS sensors are attractive as simple and effective point sensors of various physical quantities; however, the necessity of using a scanning source or an OSA noticeably increases the price of these devices. In the literature, there is a wide variety of proposed and investigated sensor configurations, which are well summarized and categorized in several reviews [42–47].

Let us conventionally list the main differences between "classic" fiber interferometric FSSs and interferometric SMS sensors. In SMS sensors, very short lengths of the MMF (typically from centimeters to several meters) are usually used, while FSSs utilize lengths up to hundreds of meters. In a basic SMS scheme (in the ideal case), several modes with an exclusively circularly symmetric field distribution ($PL_{0\mu}$ modes) are excited due to a central launch of the MMF; therefore, an interference pattern is formed as a ring-shaped structure. By contrast, in FSSs, because of their long fiber length, even a central launch leads to the formation of a speckle pattern due to power redistribution to other modes including modes with a non-zero azimuthal number (due to mode coupling). Moreover, it is usually assumed that the power is distributed among a large number of modes, so the speckle pattern consists of many interference spots. The significant fiber length in FSSs also leads to the introduction of random phase shifts to modes' phases (see Section 3). SMS sensors operate in a spectral domain, while FSSs typically work at static wavelengths. In FSSs, the entire speckle pattern is often used for signal processing, while SMS sensors use only a part (usually central) of the interferometric pattern, "accepted" by the output SMF. Taking the above into account, the theory and sensor's simulation approaches are sometimes different or focused on different aspects. For instance, in the case of SMS sensors, researchers often involve the effect of self-focusing [48]. Another example is a calculation of launching conditions in a broad spectral range in the case of SMS sensors [49], thus assuming a change in the modal power distribution (MPD) with wavelength during sensor operation (for FSSs, it is desirable to know the MPD only at the operating wavelength). Therefore, it should be emphasized that following the title of this review, in the next section, we provide a theoretical background based on a "traditional" specklegram approach.

Finally, it should be mentioned that the term "SMS", usually associated with intermodal interferometric sensors, also simply describes a fiber structure, and therefore sensors operating on principles other than interferometry are often called SMS sensors as well. This can cause a certain confusion in terminology. For example, a microbend sensor, presented in [50], consists of an SMS structure but operates as an intensity sensor with a modulated MPD.

3. Fundamentals of Optical Fiber Speckle Sensing

Optical fibers are characterized by various parameters. Among them, the parameters responsible for modal properties are mostly fiber core diameter, relative refractive index difference of the core and cladding (refractive index contrast), wavelength, and the refractive index profile of the core (the standard ones are step-index (SI) and graded-index (GI) profiles) [51]. Unlike single-mode fibers, multimode fibers (MMFs) support the propagation of many modes. Each fiber mode is characterized by its field distribution $E(r,\phi)$ in the fiber cross-section and propagation constant β, where r and ϕ are the radius and the angle of the polar coordinates in the fiber cross-section. For standard fibers, the weakly guiding approximation is applied and the basis of linearly polarized modes ($LP_{\eta\mu}$ modes, where η is the azimuthal number and μ is the radial number) is used in simulations [51–53].

The maximum number of LP modes (herein, we refer to this simply as modes) able to propagate in a fiber with given parameters is limited and can be estimated for SI and GI fibers, as presented in Equations (1) and (2), respectively,

$$M = \frac{V^2}{2}, \tag{1}$$

$$M = V^2 \left[\frac{\alpha}{2(\alpha+2)} \right], \tag{2}$$

$$V = a k_0 NA, \tag{3}$$

where V is the normalized frequency, a is the core radius, k_0 is the free-space wave number ($2\pi/\lambda$), NA is the numerical aperture of the fiber, and α is the profile parameter [51]. Depending on the launching conditions, all modes can be equally excited in the extreme

case (overfilled launch), or the power carried by each mode can vary from mode to mode, providing a particular MPD [54].

If the fiber modes are excited by a coherent light source, they interfere at the fiber end-face, forming a complex interference pattern with multiple interference peaks, which is called a speckle pattern (SP) (Figure 2). The characteristics of SPs are strongly related to the fiber parameters, including the number of excited modes and the refractive index profile. Figure 2b demonstrates the SPs recorded at the end-face of MMFs with a multimode launch provided by a mode scrambler. Generally, the higher number of excited modes provides a higher number of speckles of smaller size, while a lower number of excited modes leads to a lower number of speckles with larger size (see Figure 2b, GI cases, where the different number of excited modes is provided by different wavelengths of 0.63, 1.3, and 1.55 µm). For an SI fiber, the "boundaries" of the SP are sharp (Figure 2b, SI case) unlike the case of the GI fiber, where intensity decays while approaching the core–cladding boundary (Figure 2b, GI cases). This is according to the profile of the core refractive index. Figure 2c shows interference patterns formed in the case of an underfilled launch realized by a connection of coaxially aligned SMFs and MMFs. The presence of ring-shaped structures for the 1 m SI MMF indicates the excitation of circularly symmetric $PL_{0\mu}$ modes, which is a typical case for interferometric SMS sensors (Figure 2c, 1 m SI case). With increasing fiber length, power is redistributed to other $PL_{\eta\mu}$ modes due to mode coupling, so the intensity profile at the MMF end-face obtains the form of an SP rather than a ring-shaped structure (Figure 2, 20 m SI case). In the case of a GI MMF, the recorded intensity profile remains almost unchanged with length due to very low mode coupling in the undisturbed fiber (Figure 2c, 1 m and 20 m GI cases). The SP is stable in the absence of any EFPs, while it transforms under disturbances applied to an MMF due to different propagation constants β of fiber modes. The type of fiber interferometer utilizing the interference of propagating modes in the MMF is known as an intermodal fiber interferometer (IFI) (Figure 1a).

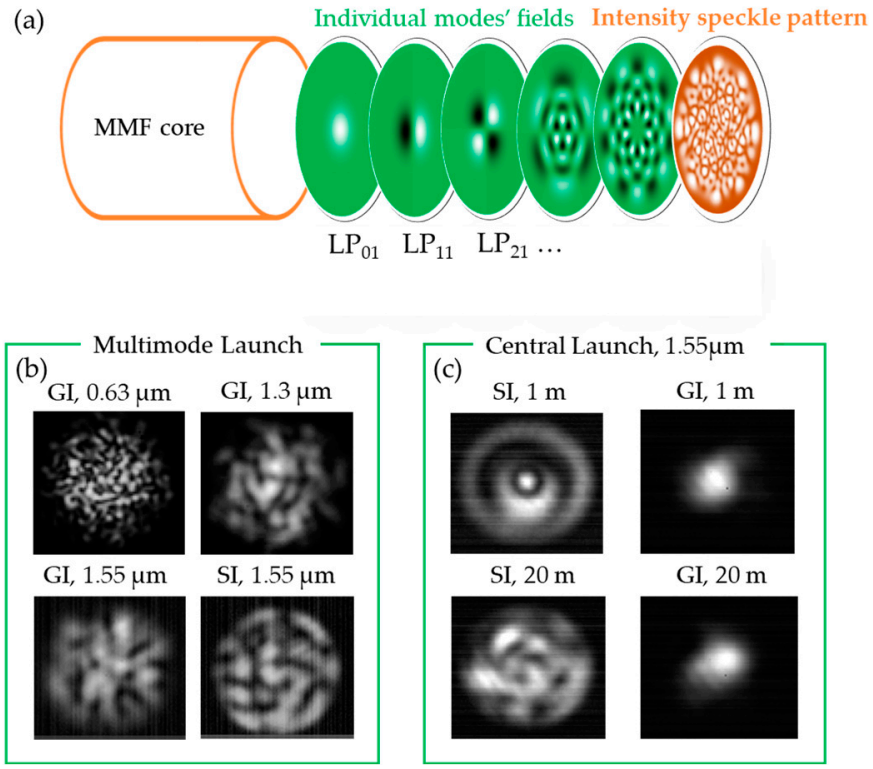

Figure 2. (**a**) Illustration of a speckle pattern formation at the end face of a GI MMF, (**b**) examples of near-field speckle patterns recorded at the end of 50 µm GI and SI MMFs at different wavelengths (multimode launch using mode scrambler), and (**c**) near-field patterns formed at the output of 50 µm GI and SI MMFs of 1 and 20 m length with underfilled launch (by centrally aligned SMF).

Due to the interferometric nature of the SP, the light intensity at a certain point (r,ϕ) of the fiber output facet can be described as [53]

$$I(r, \varphi, M, L) = \sum_{k=1}^{m} (A_k)^2 (E_k(r, \varphi))^2 + \sum_{i=2}^{m} \sum_{k=1}^{i-1} A_k A_i E_k(r, \varphi) E_i(r, \varphi) \cos[\Delta\beta_{ik} L + \Delta\phi_{ik}] \quad (4)$$

where the first term is a constant component and the second term is an interferometric component representing the sum of interferences of all pairs of excited modes, m is the number of excited modes ($2 \leq m \leq M$), L is the fiber length, A_i is the amplitude of the i-th mode, $E_i(r,\phi)$ is the mode function of the i-th mode (normalized mode field distribution), and $\Delta\beta_{ik} = \beta_i - \beta_k$ is the difference in propagation constants β of modes i and k. The cosine argument also contains a phase shift difference $\Delta\varphi_{ik} = \varphi_i - \varphi_k$, where $\varphi_{i(k)}$ is the $i(k)$-th mode's phase shift, which is usually considered random (uniformly distributed in the range of $[-\pi; \pi]$). This is due to the phases of the initial mode at the fiber input and accumulated random phase shifts obtained at some fiber inhomogeneities, bends, twists, etc. If the fiber remains static, $\varphi_{i(k)}$ remains random but static. It is also assumed in Equation (4) that the fiber is lossless and the light source is monochromatic and highly coherent; the polarization of modes is not taken into account (i.e., we use a scalar IFI model). A consideration of polarization would increase the complexity of analysis; however, the practical effect is mainly a reduction in the SP contrast, as orthogonally polarized modes do not interfere; in practice, a polarizer is often used at the output of an MMF to maximize the SP contrast [55]. The IFI signal is considered to be recorded in a near-field. The surface area of a PD is considered to be smaller or similar to the typical size of the speckles to provide maximum signal contrast and dynamic range.

If the fiber experiences external perturbation, the arguments of the cosines in Equation (4) change, leading to an SP transformation. In simulations, EFPs are often considered as changes in fiber length: $L = L_0 + \delta L$, where L_0 is the initial fiber length and δL is the fiber length alteration (deterministic value) caused by EFPs. Also, it is usually considered in simulations that the IFI signal is caused only by modal interferences but not mode coupling, mode parameter transformations, and other effects. Otherwise, the complexity of the model and simulations rises drastically. This explains the lack of theoretical models in papers related to specklegram systems, for example, with an exposed core, where contact of the core with the surrounding media can change not only the modes' phases but also local propagation constants, mode coupling coefficients, and field distributions [56].

It should be mentioned that in several works, the actual mode functions and mode amplitudes are replaced by a random value of the product $A_i E_i$ at a PD coordinate (r,ϕ) for simplicity [53]. This is substantiated by the fact that the local mode intensities are very different at the particular point of fiber cross-section even for a known MPD. The latter is due to the mode field complexity, which rises with the order of modes.

An example of an IFI signal I versus fiber elongation δL is presented in Figure 3. Here, a large δL was used to show the general dependency $I(\delta L)$. It is seen that the signal response to fiber elongation is quite complex and highly nonlinear. The complexity of the signal is conditioned by the number of pairs of interfering modes with their propagation constant differences $\Delta\beta_{ik}$, phase shifts $\Delta\varphi_{ik}$, and local products of $A_i E_i(r,\phi)$ at the PD position in the fiber cross-section. If only two modes are excited, the signal has a sine shape, while the complexity of the signal increases with the number of excited modes: each pair of interfering modes contributes with a sine-shaped signal with its period (provided by $\Delta\beta_{ik}$) and phase. Moreover, fiber rearrangement, bending, or environment condition changes will result in changes in L_0 and $\Delta\varphi_{ik}$ and, therefore, in different dependences $I(\delta L)$ in Figure 3. The IFI response can be very different at different coordinates of the SP (Figure 3a,b) that is used for signal processing such as averaging over the fiber cross-section or correlation processing (Section 4).

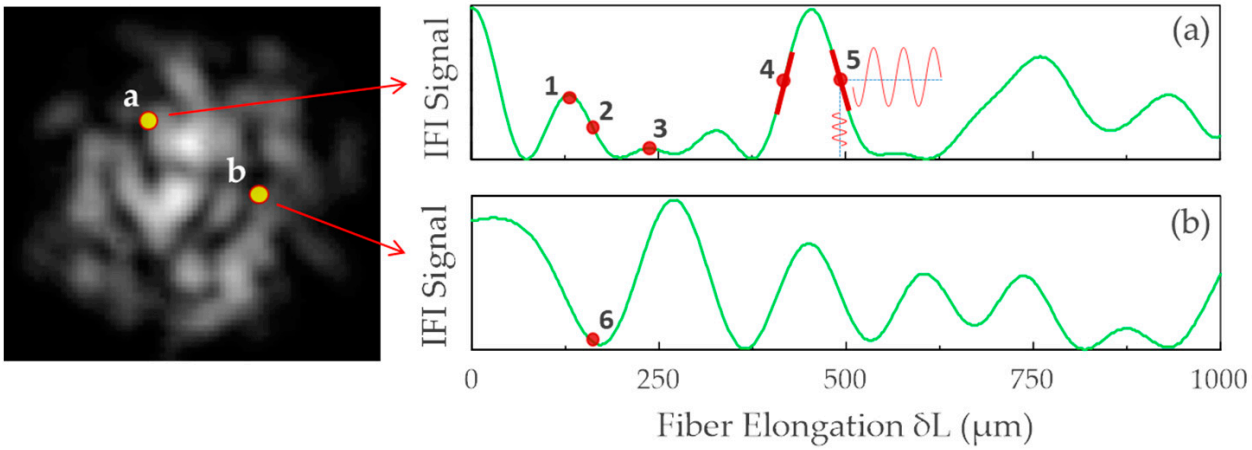

Figure 3. Illustration of IFI signal response to fiber elongation. (**a**,**b**) show that the response can be very different at different coordinates of the speckle pattern. Red points show examples of operating points for small EFPs. It is seen that points 2, 4, and 5 provide a quasi-linear response, while the response at operating points 1 and 3 will be highly nonlinear; the sensitivity at point 3 is close to zero (fading effect). Even in quasi-linear zones, the sensitivity and the dynamic range (points 2 and 5) as well as the phase of the signal (points 4 and 5) can differ. While the response is quasi-linear at one coordinate (graph (**a**), point 2), at the same time, it can be nonlinear at another coordinate (graph (**b**), point 6).

It is seen that the entire signal has certain quasi-linear zones (for example, points 2, 4, and 5 in Figure 3). On the contrary, at points 1 and 3, the response would be nonlinear. Moreover, the sensitivity at point 3 would be close to zero (fading effect). It is also seen that while the response at one coordinate of the SP is quasi-linear, at the same time, it can be nonlinear at another coordinate (points 2 and 6 in Figure 3). Even in quasi-linear zones, the sensitivity and the dynamic range (points 2 and 5) as well as the phase of the signal (points 4 and 5) can differ.

Thus, in the case of weak EFPs, a quasi-linear response can be achieved by choosing a correct operating point. However, in practice, it is very problematic to keep the operating point fixed: slowly changing environmental conditions (e.g., temperature), fiber rearrangements, and laser frequency instabilities lead to operating point drift or jumps that change sensitivity (fading effect) and a transfer function. Thus, the fundamental problems of IFIs and FSSs are signal fading, nonlinearities, and quasi-random responses in general. It should be mentioned that in several works, two mechanisms of the mode's phase difference modulation have been suggested: the first is related to the modes' optical path changes described above, and the second is related to fiber bending, twisting, and other perturbations causing a mode coupling [57–59]. In the latter case, the modulation of the phase difference of the modes occurs due to mode coupling but not due to simply δL. This complicates the analysis and makes fading behavior even more unpredictable [58]. To overcome the problems described above, various signal-processing solutions have been developed and investigated. They include averaging, correlation analysis, machine learning, and other techniques that are reviewed in Section 4.

It is seen from Equation (4) that the IFI properties (range of sensitivities, complexity of the signal, spectral components) depend on a set of parameters: mode amplitudes $A_{i(k)}$ and number of excited modes m (or MPD), a coordinate of the PD at the fiber cross-section, propagation constant differences $\Delta\beta_{ik}$, and mode field distributions $E_{i(k)}(r,\phi)$. The last two parameters ($\Delta\beta_{ik}$ and $E_{i(k)}(r,\phi)$) significantly depend on the refractive index profile of the MMF. In the case of an SI fiber, fiber modes are well approximated by Bessel modes [51,52,54], while modes of graded-index fibers are usually approximated by Laguerre–Gaussian (LG) modes [60]. For LG modes with a low radial number μ, the mode fields are "concentrated" closer to the core center, while they tend to occupy the entire physical space of the core cross-section with the rise in μ. This is not the case for Bessel modes where mode fields

occupy approximately the entire cross-section of the core (see, for example, Figure 2c). This affects the IFI properties depending on the PD position in the fiber cross-section: the averaged IFI sensitivity decreases with the displacement of the PD from the core center towards the core–cladding boundary in the case of the GI fiber [55,61].

An even more important parameter is the difference in the modes' propagation constant $\Delta\beta$. For SI fibers, propagation constant β can be calculated by solving the characteristic equation for the tangential field components at the core–cladding boundary [51,52]. In the SI case, modes have different β and disordered spacing $\Delta\beta$ between "neighbouring" modes (i.e., modes with adjacent values of β) (Figure 4a). (We note that graphs in Figure 4 are plotted using the modes' refractive index n for convenience, according to relation $\beta = 2\pi n/\lambda$; the vertical axis in Figure 4a takes into account the presence of two degenerated modes for modes with non-zero azimuthal number η.) Therefore, the interferometric signal formed by the interference of different neighboring modes (and, therefore, by other pairs of modes) will demonstrate different sensitivity, period, and beat length $\Lambda_{ik} = 2\pi/\Delta\beta_{ik}$. Note that some of the modes have very close propagation constants (Figure 4a) and, therefore, quite a long beat length (several centimeters). Thus, the resulting IFI signal $I(\delta L)$ becomes quite complex with many spectral components.

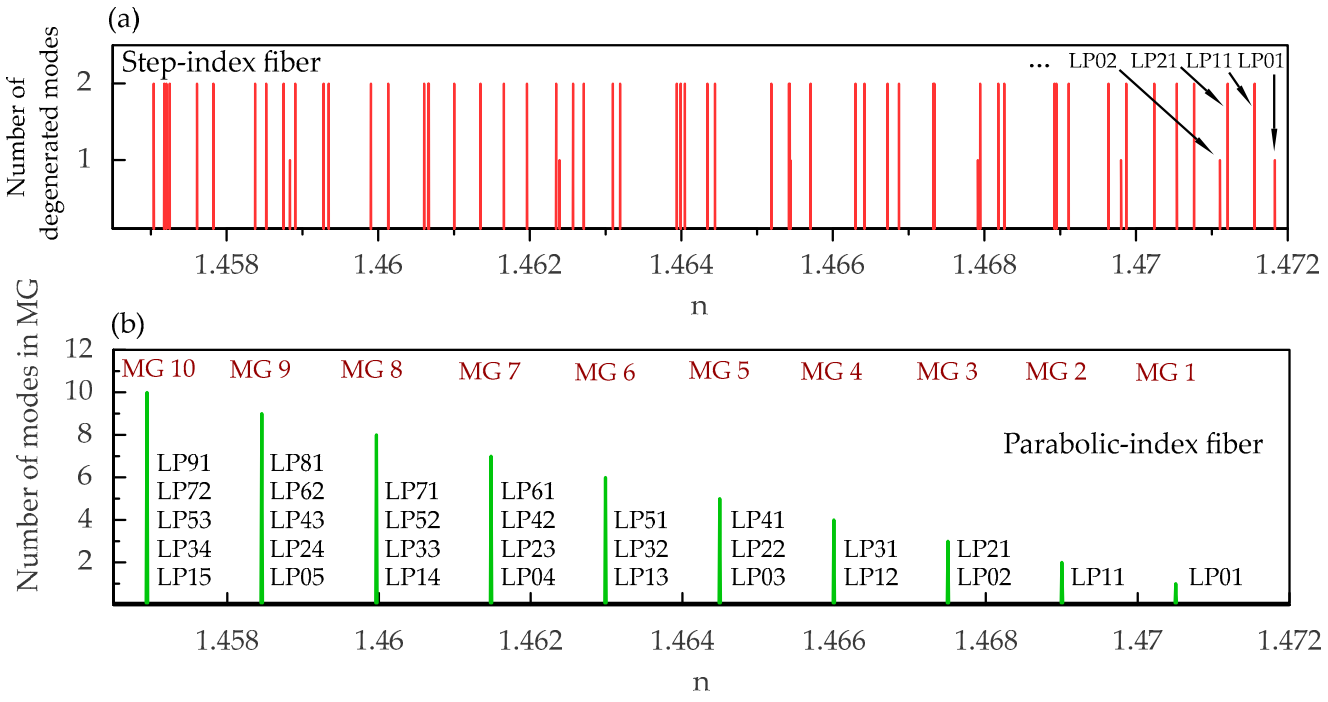

Figure 4. Refractive indices for modes of (**a**) SI and (**b**) GI ($\alpha = 2$) fiber, calculated for the fiber with parameters $a = 25$ µm, $\lambda = 1.55$ µm, $n_0 = 1.472$, and NA = 0.21. The corresponding β can be found according to the formula $\beta = 2\pi n/\lambda$. For an SI fiber, each mode has its β; the $\Delta\beta$ between adjacent modes depends on the mode numbers. For a GI fiber ($\alpha = 2$), modes are combined into mode groups (MGs); all adjacent MGs have the same $\Delta\beta$.

A completely different case takes place for the GI fiber. Here, particular sets of modes are combined into mode groups (MGs): each MG contains modes with (approximately) equal propagation constants [51,54]. Using the Wentzel–Kramers–Brillouin (WKB) approximation, the analytical expression for each MG's propagation constant can be derived [51,54,62]:

$$\beta_m = \frac{2\pi}{\lambda} n_0 \left[1 - 2\Delta \left(\frac{m_g}{M_g} \right)^{\frac{2\alpha}{\alpha+2}} \right]^{\frac{1}{2}}, \quad (5)$$

where m_g is the MG number taking integer values from 1 to M_g (index g emphasizes the modes' groups instead of separate modes), Δ is the refractive index contrast, n_0 is the core refractive index at the fiber axis, α is the profile parameter, and M_g is the maximum number of MGs able to propagate:

$$M_g = a\sqrt{\Delta}\frac{2\pi}{\lambda}n_0\sqrt{\frac{\alpha}{\alpha+2}} \tag{6}$$

The number of modes belonging to a given MG is defined by the number of combinations $(\mu; \eta)$, which can be found for a given m_g according to the formula $m_g = 2\mu + \eta - 1$. Taking into account two degenerated modes for modes with non-zero azimuthal number η, it can be seen that the number of modes belonging to an MG is equal to an MG number. The consideration of two polarization states for each mode will further double the number of modes in each MG.

An interesting case is a parabolic profile of refractive index ($\alpha = 2$) where propagation constants of MGs are equidistant (Figure 4b). This means that the interferometric signal formed by the interference of any neighboring MGs has the same period and beat length according to the same propagation constant difference of adjacent MGs $\Delta\beta_p$ (index p emphasizes the parabolic profile of refractive index). Therefore, the IFI signal $I(\delta L)$ is expected to be less complex with significantly fewer spectral components compared to the step-index case. The spectral components are equidistant as well; if all modes are excited, the first spectral component corresponds to the interference of the adjacent MGs (provided by $\Delta\beta_p$), while the last spectral component corresponds to the interference of the fundamental mode and the modes belonging to the highest-order MG (provided by the maximum $\Delta\beta_{pmax} = \Delta\beta_p(M_g - 1)$). As the propagation constants within the MGs are approximately equal, the interferometric signal formed by modes belonging to the same MG is insensitive to EFPs ($\Delta\beta_{ik} \approx 0$ in Equation (4)). Thus, in the case of the GI profile, the number of modes m in Equation (4) can represent the number of mode groups m_g, and the mode amplitudes and field distributions are those of mode groups as well.

To complete the topic of IFI signal formation, the effect of laser frequency modulation (LFM) must be discussed. Apart from the EFPs, the LFM also generates the IFI signal as $\Delta\beta_{ik}$ in Equation (4) is sensitive to optical frequency shifts $\delta\nu$. In fiber communications, this effect has been studied within the topic of modal noise [63]. To consider the LFM as a source of the IFI signal, the product $\Delta\beta_{ik}L_0$ can be decomposed into Taylor series in the vicinity of the optical frequency mean value ν_0 [53]:

$$\Delta\beta_{ki}L_0 = (\beta_k(\nu_0) - \beta_i(\nu_0))L_0 + \left(\frac{d\beta_k(\nu_0)}{d\nu} - \frac{d\beta_i(\nu_0)}{d\nu}\right)\delta\nu \cdot L_0 = (\beta_k(\nu_0) - \beta_i(\nu_0))L_0 + \left(\frac{1}{V_k} - \frac{1}{V_i}\right)\Big|_{\nu_0}\delta\nu \cdot L_0 \tag{7}$$

where $V_{i(k)}$ is the group velocity of the $i(k)$-th mode (a linear approximation was applied when decomposing into a Taylor series). It is seen that the first term in Equation (7) is fixed, while the second term is proportional to frequency shift $\delta\nu$ and fiber length L_0. Thus, the IFI sensitivity to laser frequency modulation rises with fiber length. This is a principal difference from the case of EFPs, where the IFI sensitivity depends on the fiber section subjected to the EFP but not on the entire fiber length. Also, the IFI sensitivity to LFM is radically stronger for the SI fiber compared to the GI fiber with $\alpha \approx 2$, where the mode propagation times are equalized [53,64]. Even though the LFM caused by fluctuations in laser frequency can be considered a source of noise for IFIs [65], intentional frequency modulation can be useful. It has been proposed as an averaging method of IFI signals [55] and for advanced IFI signal processing providing signal linearity and fading mitigation [66]. The LFM principle is also used in interferometric SMS sensor schemes, where periodically updating wavelength scans are used to extract the signal [42]. It should be mentioned that the mechanisms of the IFI with LFM have been utilized in other specklegram-related applications such as MMF-based spectrometers [67].

As discussed above, if no processing algorithms are used, the IFI demonstrates a quasi-random transfer function and sensitivity, the response can be highly nonlinear, and the useful signal experiences fading. This complicates both the effective sensing and the determination of the IFI properties, which depend on fiber parameters, the laser wavelength, and the MPD. To enable a convenient analysis of IFI properties, the apparatus of so-called averaged amplitude characteristics (ACs) has been developed [53]. It is based on ensemble averaging of the IFI response to EFPs and plotting the graph of the averaged standard deviation of the signal versus EFP amplitude, for example, fiber elongation δL (Figure 5a). Unaveraged ACs are quasi-random and strongly nonlinear (gray curves in Figure 5a), while the averaged AC is stable and reproducible (red dashed curve in Figure 5a). It contains a rising part and a saturation part. The saturation occurs when the EFP amplitude exceeds the maximum beat length of adjacent modes (modes with minimum $\Delta\beta$). The AC method allows for effective analysis (theoretically and experimentally) of the IFI properties depending on fiber parameters, wavelength, and MPD [35,55,61]. Figure 5b shows an example of averaged ACs for two wavelengths of 0.63 and 1.3 μm and two MPDs for the 0.63 μm wavelength. The graphs allow us to compare averaged sensitivities and to estimate a range of δL when the quasi-linear response can be achieved. In the given example, it is seen that the average sensitivity in the rising part of the curves is significantly stronger for the multimode case than for the few-mode case at 630 nm, while the multimode case at 630 nm is more sensitive to EFPs than the multimode case at 1300 nm due to a higher number of modes able to propagate at 630 nm than at 1300 nm. It should be mentioned that the quasi-linear part of the dependences ends at significantly lower EFP amplitudes for the cases with stronger sensitivities (630 nm, multimode case) than for the cases with lower sensitivities (1300 nm multimode, and 630 nm few-mode cases).

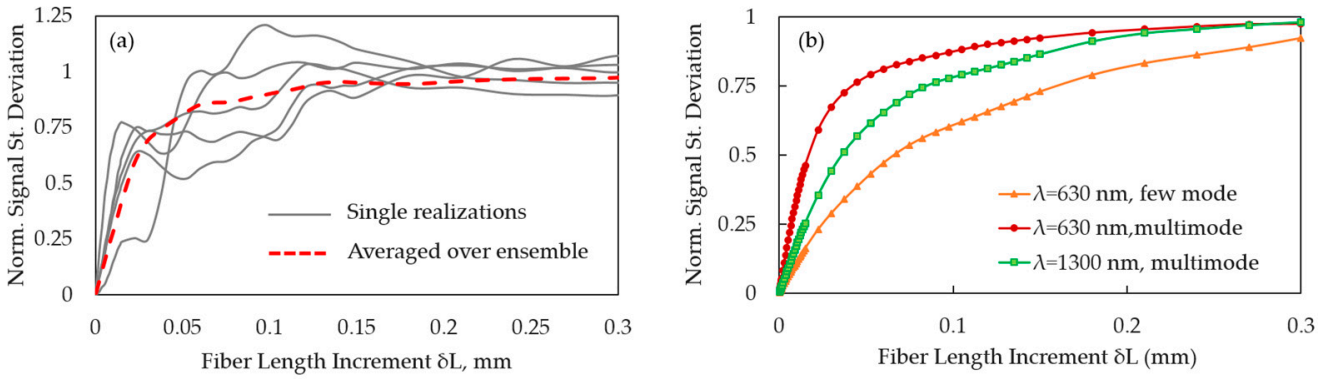

Figure 5. Example of the amplitude characteristics experimentally obtained in [55,61]: (**a**) several unaveraged ACs and the AC obtained by ensemble averaging, and (**b**) the ACs spatially averaged over fiber cross-section for two wavelengths (630 and 1300 nm) and two cases of launching conditions for 630 nm.

Further, various averaging methods have been experimentally analyzed using the AC method [55,61]. They include ensemble averaging, averaging "over long realization", laser frequency averaging, spatial averaging over the fiber cross-section, and their combinations. While the first two methods are useful for the assessment of IFI properties, the spatial and frequency averaging methods have also been used for real-time sensing applications. To complement the ACs for the EFPs of strong amplitudes, the averaged spectral characteristics (SC) have been introduced as well; thus, the IFI can be characterized by the pair of AC and SC for the full range of EFP amplitudes [53].

It should be noted that the IFI signal registration can be performed in the near-field and far-field zones. Practically, the selection of one of these two methods to use depends on the equipment and convenience: near-field registration allows us to use a camera matrix and to analyze the entire SP, but it requires the use of imaging optics (e.g., microscope objective), while registration in the far-field using one or multiple photodetectors is simpler, but it does not allow us to analyze the entire speckle pattern, rather only parts of it. For theoretical

investigations of IFIs, in particular, for the analysis of IFI characteristics depending on fiber parameters (refractive index profile, MPD, etc.), the use of the near-field is more straightforward. The far-field distribution of modes can be calculated by the Fourier transform of the near-field distribution, and the results can be different depending on the refractive index profile of the MMF [54]. It has been demonstrated that the modes' field shapes are the same for the near- and far-field for a GI profile, while they significantly differ in the case of an SI fiber [54]. The same behavior can be expected for speckle patterns.

In this section, we considered the basic physics of IFIs, and we discussed signal characteristics and limitations and the relations between fiber parameters and IFI properties. We note that the theoretical background was limited by a weakly guiding approximation and two cases of refractive index profiles (step-index and graded-index), while a great variety of specialty optical fibers can be applied for specklegram sensing. The consideration of this variety of fibers, however, would significantly complicate the theory and is beyond the scope of the format of this article. In the following sections, signal processing approaches and the FSS applications are reviewed in more detail.

4. Signal Processing and Data Analysis

In Section 3, we mentioned two main problems of FSSs: the quasi-random and nonlinear transfer function (changing under drifting environmental conditions) and, as a result, signal fading. The first problem does not allow precise measurement of EFPs; rather, the sensor can detect some events disturbing the fiber, for example, heartbeats in medical applications [68,69] or intrusion into a secured territory in perimeter surveillance applications [70]. If the interferometric signal is detected using one PD (or camera pixel), the second problem, signal fading, does not allow reliable measurement of the perturbation amplitude. Moreover, the perturbation can be completely missed, since the sensitivity can drop down to almost zero. Therefore, the main purpose of signal processing algorithms and approaches is to overcome the above problems. Researchers have been trying to reach this goal either via a spatial domain (analyzing different parts of the speckle pattern, i.e., performing multichannel signal detection and processing, or analyzing the speckle pattern as a whole), or spectral domain, using a scanning light source or broadband source with an OSA (or spectrometer). Below, various signal processing techniques are categorized and reviewed.

4.1. Intensity Approach

In the simplest case, intensity-based FSSs can be realized by receiving an intensity-modulated signal after spatial filtering of the SP using one PD. As it was mentioned above, the signal will experience nonlinearity and fading under changing environmental conditions. As a solution, multichannel signal detection provides a mitigation of fading that allows the realization of reliable threshold sensors (e.g., heartbeat monitoring, perimeter surveillance). This approach is well investigated [36,59,71]. For instance, in works [36,59], the authors compared algorithms based on calculation moduli of the signals from several photodetectors; the work [71] analyzes the influence of the number of photodetectors on the effectiveness of fading mitigation. The authors of these papers assume that the useful signal has a high-frequency spectrum compared to slowly changing (quasi-static) environmental conditions. Therefore, the signal was subjected to high-pass filtering before applying the algorithms. It should be noted that amplitude single-channel and multichannel detection (spatial filtration) can also be realized by using one or several single-mode fibers serving as spatial filters at the output of the MMF [72]. In this case, the electronic part of the scheme can be a good distance away.

A more advanced approach consists of the use of a CCD or camera matrix instead of a set of PDs [37]. This allows camera pixels to be used as separate PDs that significantly increases the number of spatial channels and, therefore, can improve the effectiveness of data processing. One camera matrix can even be used to record SPs from several MMFs simultaneously [73]. However, the use of cameras can significantly limit the bandwidth of the sensor, which can be inappropriate in some applications. Generally, the same algorithms investigated for the

case of multiple photodetectors can be applied with the use of cameras. For example, in works [37,74], the sum of absolute values of signal changes is analyzed; in work [55], the effectiveness of the averaging of signal amplitudes for fading mitigation (and, therefore, for the stability of the response) is experimentally investigated for different wavelengths (that define the maximum number of propagating modes) and MPDs. It should be mentioned that the use of the absolute value of the alternating signal (e.g., sine shape) leads to the doubling of signal spectrum width [37]. In works [69,70,75], authors applied a time differentiation of the camera pixel's signal. The work [76] demonstrates the results of the application of various image processing algorithms (both intensity-based and correlation-based) for speckle pattern processing. Authors assumed that the type of EFPs, microbends, causes not only DPM but also strong mode coupling between core modes and further between core and cladding modes. The latter means that the condition of constant total intensity at the fiber output is no more valid that was considered in the investigated processing approaches. It should be noted that authors compare the processing algorithms in terms of linearity, sensitivity, and dynamic range, while the effectiveness of fading mitigation is out of the scope of this work. In [77], the low frame rate and response time of cameras and CCD arrays usually considered as disadvantages, were proposed as a way to measure the amplitude of high-frequency EFPs by calculating the contrast of the SP: the higher the amplitude of the EFP, the lower the contrast of the SP due to averaging of the SPs over the response time of the camera matrix (a similar principle is also applied for SP elimination, i.e., minimization of the SP contrast towards zero, in MPD and encircled flux measurements).

4.2. Correlation Approach

In general, the correlation approach is based on the comparison of an SP recorded by a camera matrix at a given moment in time with a certain reference SP recorded in the absence of EFPs. In this case, the problem of signal fading is effectively solved, since the entire SP is analyzed. Several research groups have developed the SP correlation approach for FSSs. For example, work [78] demonstrates the correlation approach for the case of fiber axial strain. The authors confirmed the stability of the sensor response for different initial conditions of the SP, which indicates the robustness to signal fading. The authors also showed the influence of the radius of the analyzed part of the SP on the correlation curve, and the influence of the camera saturation on measurement errors; they demonstrated a method of increasing the sensor's dynamic range by periodically updating the reference image. In work [79], the authors considered microbend perturbations of an MMF and proposed the normalized inner product coefficient for analysis of EFPs; the "updating reference" technique was also applied for the extension of sensor's dynamic range. In work [80], the authors investigated the effectiveness of the correlation method when just a few modes were excited in an MMF; they proposed the utilization of diffusion transparency to improve the quality and stability of the measured signals (Figure 6a). In [76], the authors investigated various image processing correlation techniques for FSSs. As mentioned in the previous subsection, the authors assumed the possibility of changes in the total output power due to the possible coupling of core and cladding modes under fiber microbendings.

Various image processing techniques utilizing the correlation approach are proposed and investigated in other works as well [81,82]. For example, in paper [82], the authors propose the application of morphological image processing for strain sensing: they converted SP images into binary form and compared them with a set of reference images recorded in advance during a controlled ramp of strains applied to the fiber. This approach demonstrated an enhanced dynamic range towards stronger amplitudes of perturbations. We suppose, however, that this approach requires stable environmental conditions (temperature); otherwise, the procedure of periodical recalibration is necessary.

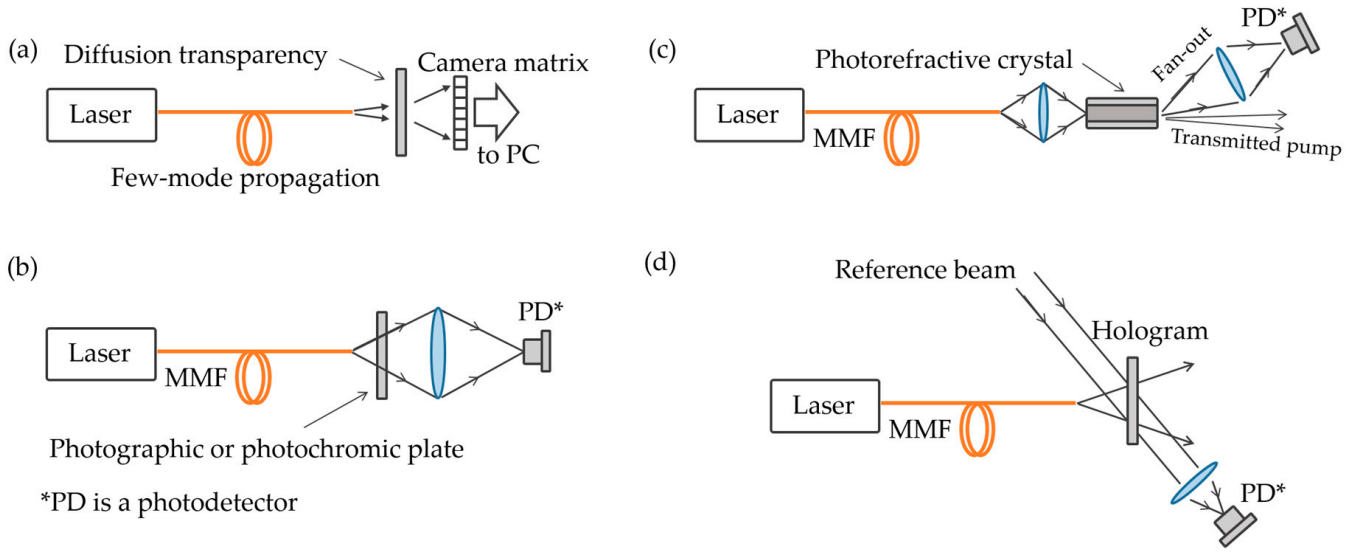

Figure 6. Variety of modified schemes for interferometric signal detection used in correlation approach of signal processing: (**a**) using a diffusion transparency in case of a few-mode propagation regime, (**b**) using a photographic or photochromic plate and a photodetector, (**c**) using a photorefractive crystal and a photodetector, and (**d**) holographic scheme with a reference laser beam.

The correlation approach can be realized not only by camera image processing, but also using a single PD. In early works [83,84], authors proposed an FSS with a photographic plate that served as an amplitude-transmission spatial filter (Figure 6b). The filter was recorded onto a photographic plate using the reference SP (in the absence of EFPs). The light that exited from the MMF and transmitted through the filter was focused into a PD. After the filter recording, the SP and the negative image in the filter were spatially matched if the fiber was undisturbed. Therefore, the PD signal was minimal. The alternation of the SP from its reference position under acoustic pressure applied to the MMF generated a PD signal proportional (under a condition of weak enough perturbations) to the acoustic pressure amplitude. This approach was attractive since it required only one PD; however, its practical use was limited since the reference SP must be unchanged and must exactly match the spatial amplitude filter, which is problematic in real conditions in the presence of temperature drift and possible fiber rearrangements. The spatial amplitude filter approach was further developed to allow its adaptive self-adjustment under slowly changing environmental conditions (and therefore under slowly transforming SP). In work [85], the authors proposed the adaptive correlation filter based on the photorefractive fanning effect (Figure 6c), while in [86], the author proposed the use of photochromic glasses for the same purpose (Figure 6b).

Finally, the holographic correlation approach has been proposed and investigated in [27]. This method provides a significant increase in the sensor's sensitivity. Notably, it exhibits potential for multiplexing capabilities through the use of reference laser beams with different angular separations or wavelengths [28]. However, since it utilizes principles of holography, it requires a reference laser beam that increases the complexity of the sensor (Figure 6d). In addition, the problem of reference SP drift under environmental conditions remains a reality.

4.3. Machine Learning Approach

The machine learning (ML) approach in FSS data processing and analysis is the newest among others. An impressive number of publications dedicated to fiber-specklegram-related applications have been published in the past few years: FSSs; MMF-based image transmission, recognition, and reconstruction; and MMF spectrometers [44,87]. Various network types, such as VGGNet, AlexNet, ANN, ResNet, and others, have been trained, and their effectiveness and reliability have been investigated for these applications. The

feature of the ML approach to FSSs is that it does not involve any theoretical basis on MMF light propagation and SP formation; it operates simply with images, being trained to recognize various scenarios of fiber perturbation from the SP evolution. FSSs studied with the use of ML include bending and curvature [88–90], tactile [91], biomedical [92], and intrusion detection [93] sensors. In several works, the investigation of the possibility of EFP localization along the MMF is presented [94–96]. In general, the ML techniques applied to FSSs have demonstrated impressive results of measurement accuracy and have opened new sensing capabilities; however, this approach also has significant practical limitations. For reliable measurements, the system must be trained for a given sample of MMF, keeping it in a particular, unchanged position, and in perfectly stabilized environmental conditions. Any fiber parameter changes (length, core diameter, refractive index profile), rearrangement, and temperature drift drastically reduce system performance. To the best of our knowledge, the ML-based FSSs resistive to environmental condition changes have still not been demonstrated. A detailed review of recent achievements of the ML application to FSSs is presented in [87].

4.4. Spectral Domain Approach

The spectral domain approach utilizes the phenomenon of the dependency of the modes' propagation constant on laser frequency (wavelength) (Section 3). As a result of different group velocities of modes, the SP is sensitive to laser frequency changes. This effect is widely used in SMS-type sensors [41]. As discussed in Section 2, the basic scheme of the SMS sensor contains a short piece of MMF sandwiched between two SMFs. Few modes in the MMF are excited by a scanning light source via the input SMF. The interferometric signal spatially filtered by the output SMF is recorded by a photodetector. As a result, a spectral response (which is a dependency of the interferometric signal versus laser frequency) of the SMS structure can be formed and updated in real-time (Figure 7). The same effect can be obtained using a broadband light source and an optical spectrum analyzer (or spectrometer). EFPs, applied to the MMF section, cause spectrum transformations. Due to a small number of excited modes and the short length of the MMF, the transmission spectrum represents a small number of interferometric maxima and minima, while spectrum transformations obtain a form of movements of the spectrum towards higher or lower wavelengths proportionally to EFPs (the shape of the spectrum remains almost unchanged). Thus, tracking a wavelength position of a spectral maximum or minimum (red arrows in Figure 7) opens a possibility for a simple measurement technique. In this case, the problem of signal fading is not explicitly present, which is a strong advantage of this sensor configuration. Also, a good linearity of the sensor response can be achieved. It should be noted that the spectral-domain SMS sensor can also be considered a set of FSSs receiving a signal via one spatial channel (output SMF fiber) and operating at different wavelengths within the range of scanning wavelength (the number of FSSs is equal to the scanning range divided by the OSA resolution or by the sampling rate of the photodetector). Interferometric time signals formed by fiber length modulation at two wavelengths λ_1 and λ_2 are schematically illustrated by black curves in Figure 7. Spectral-domain SMS sensors have a great number of variations based on fiber types, interrogation techniques, and combinations with other sensing techniques, applications, etc., that are comprehensively reviewed in several articles [42–47]. It should be noted that a potential problem of the peak-tracking technique can occur in the case of a highly multimode propagation regime and long lengths of MMFs increasing the sensor's sensitivity. Here, spectrum transformation ceases to represent simply shifts towards higher and lower wavelengths, but obtains more complicated behavior, changing the shape of the spectrum. Therefore, peaks that are supposed to be tracked can appear and disappear, and their tracking becomes impossible.

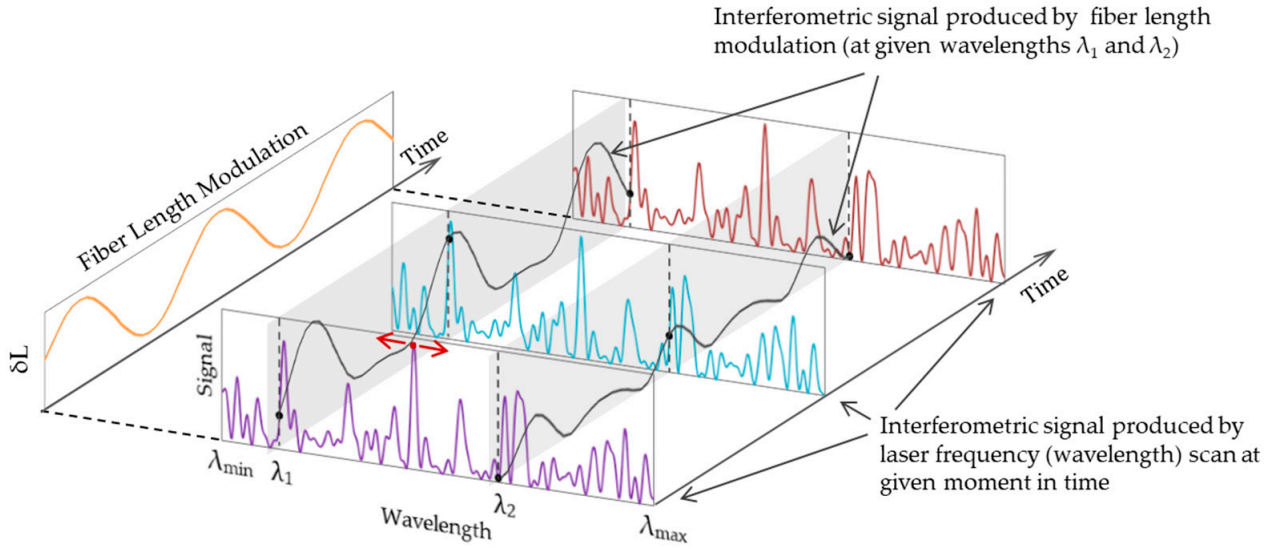

Figure 7. Schematic illustration of spectral-domain intermodal fiber interferometer signal. The signal is formed by continuously updated wavelength scans. Measurements can be performed by the tracking of some interferometric peak shifting under EFPs (red arrows). The scheme can also be considered a set of interferometers operating at different wavelengths (black curves at λ_1 and λ_2).

Another promising approach that can be used instead of spectral peak tracking is the analysis of the fast Fourier transform (FFT) of the SMS transmission spectrum. The FFT spectrum of continuously updating wavelength scans demonstrates several spectral peaks (harmonics); each harmonic corresponds to a particular pair of interfering modes. Thus, by analyzing the phase on the frequency of the particular harmonic, one can measure EFPs [97–101]. This approach provides a linear relation between the phase and EFPs, which is a strong advantage. The sensor's dynamic range can be extended towards strong perturbations by implementing a phase unwrapping technique. Phase demodulation for SMS structures with a length of the MMF section up to 50 m (GI MMF, few-mode regime) has been demonstrated [102]. However, obtaining reliable results, as well as in the previous technique of peak tracking, becomes more complicated with the increasing number of excited modes, since the spectral components corresponding to different pairs of interfering modes can be very close to each other and even overlap, making the phase tracking of harmonics unreliable.

One more approach proposed for a spectral domain FSS consists of the use of the auto-correlation function of the spectral interferometric signal [66]. The correlation coefficient is calculated between the reference wavelength scan, which is recorded under the absence of EFPs, and the signal scan, updating in real-time and transforming under EFPs. This approach can be considered an alternative to the correlation processing of the specklegram image described in Section 4.2; however, it allows for obtaining a linear sensor response by applying a certain wavelength shift to the reference scan, thus shifting the operating point to a linear part of the correlation function. This approach confirmed its reliability even with the highly multimode regime of the GI MMF.

5. Sensing Applications

Optical fiber specklegram sensors have proven their capability in measuring a diverse array of parameters, including micro-bending, strain, vibration, temperature, and refractive index. These sensors find applications in various sectors such as healthcare, structural health monitoring, and security or surveillance.

The sensing parameters can be categorized into two main groups, i. physical and ii. chemical parameters, as summarized in Table 1. Within the physical parameters group, we can include strain, pressure, vibration, sound, bending, and temperature. On the other hand,

the second group primarily focuses on liquid or gas measurements, where light must physically interact with the ambient environment, encompassing refractive index and relative humidity.

Table 1. Categorization of the different basic parameters, which can be measured using optical fiber sensors.

Group A—Physical	Group B—Chemical
Strain	Refractive index
Temperature	Relative Humidity
Pressure	Gas sensing
Curvature	pH
Vibrations	

Regarding the materials used in developing these sensors, the main types are silica and polymer fibers. It is noteworthy that depending on the material, certain parameters may transition from one group to another. For example, many polymers exhibit hydrophilic characteristics, enabling a mechanism where the polymer absorbs water content, causing the fiber to swell. This swelling can lead to local expansion of the fiber dimensions. In cases where only the cladding of the fiber absorbs water, pressure is applied to the core. Consequently, fluctuations in relative humidity can be directly detected through strain or pressure sensitivity.

Figure 8 illustrates these two main categories of sensing parameters, physical and chemical, and also shows an overlapping area where some chemical parameters can be measured indirectly through physical parameters. For example, the relative humidity concentration can be measured indirectly when a hydrophilic material absorbs the water content and swells. As a result, a strain is applied to the fiber core.

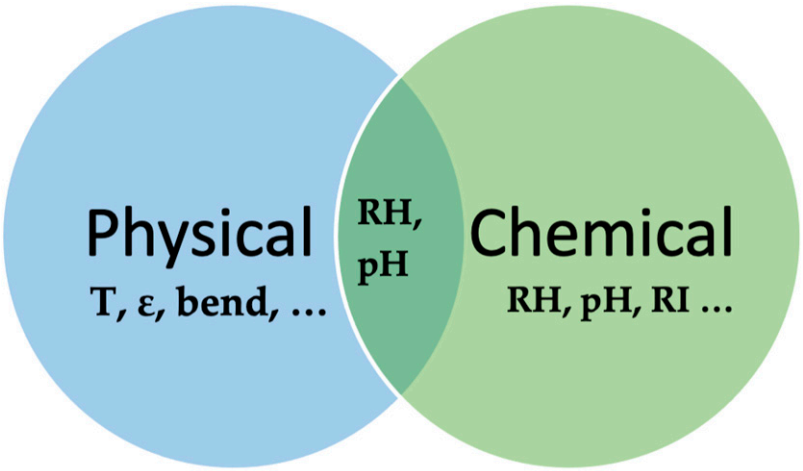

Figure 8. Schematic diagram of the categorization of the different sensing parameters that can be measured using optical fiber sensors.

In FSSs designed for physical parameters (group A), the sensing mechanism and sensitivity are conditioned only by properties of the fiber (possible number of propagating modes, refractive index profile, fiber material, elasticity, Young's modulus, strain-optic coefficient, thermal expansion, and thermo-optic coefficients). As a result, the sensing procedure and analysis are more straightforward. On the other hand, for the measurement of parameters of group B, the fiber needs to be specifically designed to make light in the fiber core interact with the ambient environment. Such specialty fiber solutions include designing fibers with an exposed core or fiber tapers, designing them to be side-polished or coreless, among others. In most cases, the second group of sensors has been realized in the form of spectral-domain SMS sensor [42]. However, sensor designs utilizing a static wavelength and analyzing the entire speckle pattern have been investigated as well [103].

As mentioned in Section 2, the very early FSS works were dedicated to acoustic and hydroacoustic sensing [31–33,83]. Further, the scope of potential applications expanded towards vibration measurement [37] and perimeter surveillance [104]. These applications as well as new directions have also been investigated in the following years: vibration [105], intrusion detection [70], security of museum collections [72], temperature sensors [106–108], strain [109,110], force sensors [111,112], tactile sensors for human–system interaction applications [111,113], monitoring of gas leakage along the pipelines [114], current sensors [115], displacement sensors [116–119], and bending sensors [120].

From the 2010s, medical applications of FSSs, especially the topic of vital sign monitoring, became quite popular in the research community: human movement detection, and heartbeat rate and breath rate measurements [68,69,121,122]. Indeed, these measurands produce event-like (pulsed) signals that can be easily detected by FFSs with simple signal processing. Recently, the topic has been extended to other applications such as pulse wave velocity monitoring [123], blood pressure monitoring [124], and blood glucose sensing [92].

In recent years, significant attention has been paid to specklegram chemical- and biosensors involving various specialty fibers or standard fiber pre-processing, allowing light interaction with surrounding media. The applications of chemical sensors include salinity sensors [125,126], refractive index sensors [103,127–132], biosensors [133], and even DNA-related sensors [134].

Finally, we would like to mention some other fiber-speckle-related applications whose principle of operation involved intermodal interference effects: fiber spectrometers [135–137], optical tweezers [138,139], and estimation of MMF bandwidth [140,141].

6. Challenges and Future Directions

Fiber specklegram sensing has emerged as a promising low-cost technique that demonstrated a potential for application in various fields, from physical (strain, vibration, temperature, etc.) to chemical applications. As demonstrated in previous sections, the main challenges of FSSs are the quasi-random nonlinear transfer function and signal fading. We described existing solutions for overcoming these main problems. The problem of signal fading has been effectively solved for highly multimode regimes utilizing multichannel signal processing and by correlation processing of SPs or in the spectral domain. The problem of the stable linear transfer function seems more complicated, and it has been solved with several limitations usually related to the dynamic range of the linear response. At the same time, spectral-domain SMS sensors demonstrate good linearity. However, the length of a sensitive element can be a restriction for some applications in the form of limited sensitivity, limited dynamic range, and the inability to distribute sensing.

On the other hand, for some recent applications of FSSs, especially utilizing specialty fibers, the problem of fading is less critical. For example, for refractive index measurement, it is necessary to record a reference SP and then perform contact with the measured liquid. This requires quite a short time, during which the environmental conditions are expected to be stable enough and will not provoke noticeable additional transformations of the SP. Thus, a correlation approach can be effectively applied in this case. One of the improvements for FSS performance seems to be a selection of fibers with low-temperature cross-sensitivity: temperature-insensitive fibers could be a solution for strain-related applications with enhanced stability [142].

One of the significant challenges and a prospective research direction is the problem of spatially resolvable distributed measurements. The topic of external impact localization has been addressed in several works. Some early solutions dedicated to intrusion detection applications consisted of simultaneously using several separate FSSs covering different zones, so the perturbation location can be found by analyzing all FSSs together [143]. Another approach for the same application also utilized multiple FSSs and involved the mechanical isolation of specific parts of MMFs [104]. The patent [144] describes a distributed sensor where the EFP localization is realized using time-multiplexing based on measurements of

the time of flight of light impulses (that should significantly increase the sensor's cost), and the specklegram technique is mentioned as one of the possible sensing principles.

Recent works involving machine learning approaches have also addressed the EFP localization problem [94–96] with promising results for identifying the EFP's location for up to 10 fiber sections. However, as discussed in Section 4.3, the main limitation of the practical application of the machine learning method is the requirement of perfect stability of the setup. Therefore, more research should be focused on obtaining reliable results under changing environmental conditions, fiber rearrangements, laser frequency drift, and other factors leading to SP transformations.

Another concept proposed as a localization problem solution suggests the use of changing the number of propagating modes along the GI MMF. It was found that the sensitivity of the FSS depends on the number of interfering modes at the location of perturbation, while the SP can be formed by a significantly higher number of modes [34,145]. Therefore, if the experimental setup provides an increasing number of excited modes along the MMF using mode controllers or the mode coupling effect, the sensitivity of the output SP will depend on the number of excited modes at the perturbation location. The proof of concept has been realized with three MMF segments and several FSS schemes, including two counter-propagating light beams (bi-directional scheme) [146,147] or two co-propagating beams at two different wavelengths [148]. In both cases, two SPs were simultaneously analyzed and by comparing the amplitude of the recorded SP signals, the place of perturbation can be found. Air gaps between MMFs [147,148], as well as long-period gratings [149], have been tested as mode controllers. Moreover, by applying spatial averaging or a correlation approach for signal amplitude determination, the system becomes robust to changing environmental conditions, i.e., becomes fading-free. However, this approach has two main factors that would limit the number of resolvable fiber segments: a limited number of mode groups in the GI MMF and difficulties with the selective modal launch and their transformations; in practice, modes are excited not stepwise, but as a certain MPD containing a set of modes with different amplitudes.

In addition to the prospects described above, the development of the FSS topic could evolve towards the application of various types of specialty multimode fibers that can exhibit new sensing features [56,103,150]. Also, combinations of different signal processing methods (e.g., spectral domain approach and multichannel signal processing with analysis of the entire SP) could provide new measurement capabilities such as enhanced linearity, EFP localization, and multiparameter sensing. The latter can also be achieved by combining FSSs with other sensing techniques, e.g., fiber Bragg gratings (this is already widely implemented for short-length spectral-domain SMS sensors [42,44]). Advanced data processing methodologies, including machine learning and AI, are crucial for improving measurement accuracy and real-time decision making. The development of algorithms resistant to changing mechanical conditions of the MMF and changing environmental conditions would radically improve the efficiency of the machine learning and AI approaches.

7. Conclusions

While fiber specklegram sensing has achieved significant milestones, acknowledging current challenges and charting future directions are imperative for its sustained success. This field holds significant potential, promising substantial contributions to industrial applications due to its simplicity and low cost. Consequently, it remains an exciting area for continuous research and innovation. As technology evolves, the integration of fiber specklegram sensing into various applications could soon become commonplace, ushering in advancements across diverse fields, from healthcare to infrastructure monitoring.

In conclusion, the trajectory of fiber specklegram sensing is poised for transformative enhancements, driven by a synergy of cutting-edge technologies. The incorporation of machine learning and artificial intelligence emerges as a pivotal force, refining speckle pattern analysis, improving measurement accuracy, and expediting decision-making processes. Moreover, the integration with other sensing elements holds the promise of fostering a

comprehensive understanding of systems, expanding the application scope in complex environments. As advancements in miniaturization techniques unfold, the prospect of more compact and portable fiber specklegram sensing devices takes center stage, unlocking transformative applications, especially in medical procedures and on-site diagnostics. The embracement of robustness, adaptability, and technological innovation is certain to propel fiber speckle sensing to new frontiers of capability and utility.

Author Contributions: Conceptualization, A.T. and I.C.; writing—original draft preparation, A.T. and I.C.; writing—review and editing, A.T., I.C., A.S. and P.M.; funding acquisition, A.T. All authors have read and agreed to the published version of the manuscript.

Funding: This research was funded by the Research and Innovation Foundation (RIF) of Cyprus under the project POLYMEROSCOPY(CULTURE/AWARD-YR/0421B/0004).

Data Availability Statement: Not applicable.

Conflicts of Interest: Author Antreas Theodosiou was employed by the company Photonics Research Center (PRC), Lumoscribe Ltd. The remaining authors declare that the research was conducted in the absence of any commercial or financial relationships that could be construed as a potential conflict of interest.

References

1. Theodosiou, A.; Kalli, K. Recent trends and advances of fibre Bragg grating sensors in CYTOP polymer optical fibres. *Opt. Fiber Technol.* **2020**, *54*, 102079. [CrossRef]
2. Mizuno, Y.; Theodosiou, A.; Kalli, K.; Liehr, S.; Lee, H.; Nakamura, K. Distributed polymer optical fiber sensors: A review and outlook. *Photonics Res.* **2021**, *9*, 1719–1733. [CrossRef]
3. Sabri, N.; Aljunid, S.A.; Salim, M.S.; Ahmad, R.B.; Kamaruddin, R. Toward Optical Sensors: Review and Applications. *J. Phys. Conf. Ser.* **2013**, *423*, 012064. [CrossRef]
4. Poeggel, S.; Tosi, D.; Duraibabu, D.; Leen, G.; McGrath, D.; Lewis, E. Optical Fibre Pressure Sensors in Medical Applications. *Sensors* **2015**, *15*, 17115–17148. [CrossRef] [PubMed]
5. Leal-Junior, A.G.; Diaz, C.A.; Avellar, L.M.; Pontes, M.J.; Marques, C.; Frizera, A. Polymer Optical Fiber Sensors in Healthcare Applications: A Comprehensive Review. *Sensors* **2019**, *19*, 3156. [CrossRef] [PubMed]
6. Xiao, G.; Guo, H.; Mrad, N.; Rocha, B.; Sun, Z. Towards the simultaneous monitoring of load and damage in aircraft structures using fiber Bragg grating sensors. In Proceedings of the OFS2012 22nd International Conference on Optical Fiber Sensors, Beijing, China, 14–19 October 2012; Volume 8421, p. 8421BD-8421BD–4. [CrossRef]
7. Theodosiou, A.; Komodromos, M.; Kalli, K. Carbon cantilever beam health inspection using a polymer fiber bragg grating array. *J. Light. Technol.* **2017**, *36*, 986–992. [CrossRef]
8. André, P.; Varum, H.; Antunes, P.; Ferreira, L.; Sousa, M. Monitoring of the concrete curing process using plastic optical fibers. *Measurement* **2012**, *45*, 556–560. [CrossRef]
9. Theodosiou, A.; Savva, P.; Mendoza, E.; Petrou, M.F.; Kalli, K. In-Situ Relative Humidity Sensing for Ultra-High-Performance Concrete Using Polymer Fiber Bragg Gratings. *IEEE Sens. J.* **2021**, *21*, 16086–16092. [CrossRef]
10. Leal-Junior, A.G.; Theodosiou, A.; Diaz, C.R.; Marques, C.; Pontes, M.J.; Kalli, K.; Frizera, A. Simultaneous measurement of axial strain, bending and torsion with a single fiber bragg grating in cytop fiber. *J. Light. Technol.* **2019**, *37*, 971–980. [CrossRef]
11. Leal-junior, A.G. Polymer Optical Fiber Sensors for Healthcare Devices: From Material Analysis to Practical Applications. Ph.D. Thesis, Digital Repository of the Universidade Federal do Espírito Santo, Vitória, Brasil, 2018; p. 201.
12. Domingues, M.F.; Tavares, C.; Leitão, C.; Frizera-Neto, A.; Alberto, N.; Marques, C.; Radwan, A.; Rodriguez, J.; Postolache, O.; Rocon, E.; et al. Insole optical fiber Bragg grating sensors network for dynamic vertical force monitoring. *J. Biomed. Opt.* **2017**, *22*, 091507. [CrossRef]
13. Chiavaioli, F.; Baldini, F.; Tombelli, S.; Trono, C.; Giannetti, A. Biosensing with optical fiber gratings. *Nanophotonics* **2017**, *6*, 663–679. [CrossRef]
14. Pospori, A.; Webb, D.J. Stress Sensitivity Analysis of Optical Fiber Bragg Grating-Based Fabry–Pérot Interferometric Sensors. *J. Light. Technol.* **2017**, *35*, 2654–2659. [CrossRef]
15. Teng, C.; Min, R.; Zheng, J.; Deng, S.; Li, M.; Hou, L.; Yuan, L. Intensity-Modulated Polymer Optical Fiber-Based Refractive Index Sensor: A Review. *Sensors* **2021**, *22*, 81. [CrossRef] [PubMed]
16. Lee, H.; Hayashi, N.; Mizuno, Y.; Nakamura, K. Slope-Assisted Brillouin Optical Correlation-Domain Reflectometry Using Polymer Optical Fibers with High Propagation Loss. *J. Light. Technol.* **2017**, *35*, 2306–2310. [CrossRef]
17. Theodosiou, A.; Kalli, K. All-in-Fiber Cladding Interferometric and Bragg Grating Components Made via Plane-by-Plane Femtosecond Laser Inscription. *J. Light. Technol.* **2019**, *37*, 4864–4871. [CrossRef]
18. Efendioglu, H.S. A Review of Fiber-Optic Modal Modulated Sensors: Specklegram and Modal Power Distribution Sensing. *IEEE Sens. J.* **2017**, *17*, 2055–2064. [CrossRef]

19. Puttnam, B.J.; Rademacher, G.; Luís, R.S. Space-division multiplexing for optical fiber communications. *Optica* **2021**, *8*, 1186–1203. [CrossRef]
20. Ukil, A.; Braendle, H.; Krippner, P. Distributed Temperature Sensing: Review of Technology and Applications. *IEEE Sens. J.* **2012**, *12*, 885–892. [CrossRef]
21. Ding, Z.; Wang, C.; Liu, K.; Jiang, J.; Yang, D.; Pan, G.; Pu, Z.; Liu, T. Distributed Optical Fiber Sensors Based on Optical Frequency Domain Reflectometry: A review. *Sensors* **2018**, *18*, 1072. [CrossRef]
22. Leal-Junior, A.G.; Theodosiou, A.; Min, R.; Casas, J.; Diaz, C.R.; Dos Santos, W.M.; Pontes, M.J.; Siqueira, A.A.G.; Marques, C.; Kalli, K.; et al. Quasi-Distributed Torque and Displacement Sensing on a Series Elastic Actuator's Spring Using FBG Arrays Inscribed in CYTOP Fibers. *IEEE Sens. J.* **2019**, *19*, 4054–4061. [CrossRef]
23. Sanders, W.C. *Basic Principles of Nanotechnology*; CRC Press: Boca Raton, FL, USA, 2018. [CrossRef]
24. Theodosiou, A.; Komodromos, M.; Kalli, K. Accurate and Fast Demodulation Algorithm for Multipeak FBG Reflection Spectra Using a Combination of Cross Correlation and Hilbert Transformation. *J. Light. Technol.* **2017**, *35*, 3956–3962. [CrossRef]
25. Leal-Junior, A.; Frizera-Neto, A.; Marques, C.; Pontes, M.J. Measurement of Temperature and Relative Humidity with Polymer Optical Fiber Sensors Based on the Induced Stress-Optic Effect. *Sensors* **2018**, *18*, 916. [CrossRef]
26. Bilro, L.; Alberto, N.; Pinto, J.L.; Nogueira, R. Optical Sensors Based on Plastic Fibers. *Sensors* **2012**, *12*, 12184–12207. [CrossRef]
27. Wu, S.; Yin, S.; Yu, F.T.S. Sensing with fiber specklegrams. *Appl. Opt.* **1991**, *30*, 4468–4470. [CrossRef]
28. Wu, S.; Yin, S.; Rajan, S.; Yu, F.T.S. Multichannel sensing with fiber specklegrams. *Appl. Opt.* **1992**, *31*, 5975–5983. [CrossRef]
29. Takahara, H. Visibility of speckle patterns: Effect of the optical guide length in coherent light. *Appl. Opt.* **1976**, *15*, 609–610. [CrossRef]
30. Crosignani, B.; Daino, B.; Di Porto, P. Speckle-pattern visibility of light transmitted through a multimode optical fiber. *J. Opt. Soc. Am.* **1976**, *66*, 1312–1313. [CrossRef]
31. Kingsley, S.; Davies, D. Multimode optical-fibre phase modulators and discriminators: I-theory. *Electron. Lett.* **1978**, *14*, 322–324. [CrossRef]
32. Layton, M.R.; Bucaro, J.A. Optical fiber acoustic sensor utilizing mode-mode interference. *Appl. Opt.* **1979**, *18*, 666–670. [CrossRef]
33. Bucaro, J.A.; Dardy, H.D.; Carome, E.F. Optical fiber acoustic sensor. *Appl. Opt.* **1977**, *16*, 1761–1762. [CrossRef]
34. Kotov, O.; Chapalo, I.; Medvedev, A. *Mode-Mode Interference Sensor with Increasing Number of Modes along the Multimode Optical Fiber*; SPIE Optical Engineering + Applications: San Diego, CA, USA, 2014; p. 92030B. [CrossRef]
35. Chapalo, I.; Theodosiou, A.; Kalli, K.; Kotov, O. Multimode Fiber Interferometer Based on Graded-Index Polymer CYTOP Fiber. *J. Light. Technol.* **2020**, *38*, 1439–1445. [CrossRef]
36. Kotov, O.I.; Kosareva, L.I.; Liokumovich, L.B.; Markov, S.I.; Medvedev, A.V.; Nikolaev, V.M. Multichannel signal detection in a multimode optical-fiber interferometer: Ways to reduce the effect of amplitude fading. *Tech. Phys. Lett.* **2000**, *26*, 844–848. [CrossRef]
37. Spillman, W.B.; Kline, B.R.; Maurice, L.B.; Fuhr, P.L. Statistical-mode sensor for fiber optic vibration sensing uses. *Appl. Opt.* **1989**, *28*, 3166–3176. [CrossRef]
38. Petrov, A.; Bisyarin, M.; Kotov, O.I. Broadband intermodal fiber interferometer for sensor application: Fundamentals and simulator. *Appl. Opt.* **2022**, *61*, 6544–6552. [CrossRef]
39. Petrov, A.V.; E Chapalo, I.; I Kotov, O. Theoretical analysis of averaging methods for intermodal fiber interferometer. *J. Phys. Conf. Ser.* **2019**, *1326*, 012023. [CrossRef]
40. Petrov, A.; Chapalo, I.; Kotov, O. *Intermodal Fiber Interferometer with Scanning Laser and Correlation Signal Processing: An Experimental Study*; Springer: Cham, Switzerland, 2021; pp. 307–316.
41. Mehta, A.; Mohammed, W.; Johnson, E.G. Multimode interference-based fiber-optic displacement sensor. *IEEE Photonics Technol. Lett.* **2003**, *15*, 1129–1131. [CrossRef]
42. Wu, Q.; Qu, Y.; Liu, J.; Yuan, J.; Wan, S.-P.; Wu, T.; He, X.-D.; Liub, B.; Liuc, D.; Ma, Y.; et al. Singlemode-Multimode-Singlemode Fiber Structures for Sensing Applications—A Review. *IEEE Sens. J.* **2021**, *21*, 12734–12751. [CrossRef]
43. Wang, K.; Dong, X.; Kohler, M.H.; Kienle, P.; Bian, Q.; Jakobi, M.; Koch, A.W. Advances in Optical Fiber Sensors Based on Multimode Interference (MMI): A Review. *IEEE Sens. J.* **2021**, *21*, 132–142. [CrossRef]
44. Wang, K.; Mizuno, Y.; Dong, X.; Kurz, W.; Koehler, M.; Kienle, P.; Lee, H.; Jakobi, M.; Koch, A.W. Multimode optical fiber sensors: From conventional to machine learning-assisted. *Meas. Sci. Technol.* **2024**, *35*, 022002. [CrossRef]
45. Wang, P.; Zhao, H.; Wang, X.; Farrell, G.; Brambilla, G. A Review of Multimode Interference in Tapered Optical Fibers and Related Applications. *Sensors* **2018**, *18*, 858. [CrossRef] [PubMed]
46. Guzmán-Sepúlveda, J.R.; Guzmán-Cabrera, R.; Castillo-Guzmán, A.A. Optical Sensing Using Fiber-Optic Multimode Interference Devices: A Review of Nonconventional Sensing Schemes. *Sensors* **2021**, *21*, 1862. [CrossRef] [PubMed]
47. Frazão, O.; Silva, S.O.; Viegas, J.; Ferreira, L.A.; Araújo, F.M.; Santos, J.L. Optical fiber refractometry based on multimode interference. *Appl. Opt.* **2011**, *50*, E184–E188. [CrossRef]
48. Wang, P.; Brambilla, G.; Ding, M.; Semenova, Y.; Wu, Q.; Farrell, G. Investigation of single-mode–multimode–single-mode and single-mode–tapered-multimode–single-mode fiber structures and their application for refractive index sensing. *J. Opt. Soc. Am. B* **2011**, *28*, 1180–1186. [CrossRef]
49. Kumar, A.; Varshney, R.K.; Antony, C.S.; Sharma, P. Transmission characteristics of SMS fiber optic sensor structures. *Opt. Commun.* **2003**, *219*, 215–219. [CrossRef]

50. Donlagic, D.; Culshaw, B. Microbend sensor structure for use in distributed and quasi-distributed sensor systems based on selective launching and filtering of the modes in graded index multimode fiber. *J. Light. Technol.* **1999**, *17*, 1856–1868. [CrossRef]
51. Gowar, J. *Optical Communication Systems*; Prentice/Hall International: London, UK, 1984.
52. Gloge, D. Weakly Guiding Fibers. *Appl. Opt.* **1971**, *10*, 2252–2258. [CrossRef]
53. Kotov, O.I.; Bisyarin, M.A.; Chapalo, I.E.; Petrov, A.V. Simulation of a multimode fiber interferometer using averaged characteristics approach. *J. Opt. Soc. Am. B* **2018**, *35*, 1990–1999. [CrossRef]
54. Hallam, A. *Mode Control in Multimode Optical Fiber and Its Applications*; Aston University: Birmingham, UK, 2007.
55. Chapalo, I.; Petrov, A.; Bozhko, D.; Bisyarin, M.A.; Kotov, O.I. Averaging Methods for a Multimode Fiber Interferometer: Experimental and Interpretation. *J. Light. Technol.* **2020**, *38*, 5809–5816. [CrossRef]
56. Cabral, T.D.; Fujiwara, E.; Warren-Smith, S.C.; Ebendorff-Heidepriem, H.; Cordeiro, C.M.B. Multimode exposed core fiber specklegram sensor. *Opt. Lett.* **2020**, *45*, 3212–3215. [CrossRef]
57. Taylor, H. Bending effects in optical fibers. *J. Light. Technol.* **1984**, *2*, 617–628. [CrossRef]
58. Kosareva, L.I.; Kotov, O.I.; Liokumovich, L.B.; Markov, S.I.; Medvedev, A.V.; Nikolaev, V.M. Two mechanisms of phase modulation in multimode fiber-optic interferometers. *Tech. Phys. Lett.* **2000**, *26*, 70–74. [CrossRef]
59. Kotov, O.I.; Liokumovich, G.B.; Markov, S.I. *Registration of Influence on Optical Fiber by Mode-Mode Interference*; Lasers for Measurements and Information Transfer: St. Petersburg, Russia, 2004; pp. 91–102.
60. Berdagué, S.; Facq, P. Mode division multiplexing in optical fibers. *Appl. Opt.* **1982**, *21*, 1950–1955. [CrossRef] [PubMed]
61. Chapalo, I.; Petrov, A.; Bozhko, D.; Bisyarin, M.; Kotov, O. Methods of signal averaging for a multimode fiber interferometer: An experimental study. In *Optical Sensors 2019*; SPIE Optics + Optoelectronics: Prague, Czech Republic, 2019; p. 110282Q. [CrossRef]
62. Marcuse, D. *Light Transmission Optics*; Van Nostrand Reinhold Company: New York, NY, USA, 1982.
63. Rawson, E.G.; Goodman, J.W.; Norton, R.E. Frequency dependence of modal noise in multimode optical fibers. *J. Opt. Soc. Am.* **1980**, *70*, 968–976. [CrossRef]
64. Kotov, O.I.; Chapalo, I.E.; Petrov, A.V. Signals of an intermodal fiber interferometer induced by laser frequency modulation. *Tech. Phys. Lett.* **2016**, *42*, 11–14. [CrossRef]
65. Kotov, O.; Chapalo, I. *Signal-to-Noise Ratio for Mode-Mode Fiber Interferometer*; SPIE Optical Metrology: Munich, Germany, 2017; p. 1032945. [CrossRef]
66. Petrov, A.; Chapalo, I.E.; Bisyarin, M.; Kotov, O.I. Intermodal fiber interferometer with frequency scanning laser for sensor application. *Appl. Opt.* **2020**, *59*, 10422–10431. [CrossRef] [PubMed]
67. Redding, B.; Popoff, S.M.; Cao, H. All-fiber spectrometer based on speckle pattern reconstruction. *Opt. Express* **2013**, *21*, 6584–6600. [CrossRef] [PubMed]
68. Lomer, M.; Rodriguez-Cobo, L.; Revilla, P.; Herrero, G.; Madruga, F.; Lopez-Higuera, J.M. Speckle POF Sensor for Detecting Vital Signs of Patients. In Proceedings of the OFS2014 23rd International Conference on Optical Fiber Sensors, Santander, Spain, 2–6 June 2014; p. 91572I. [CrossRef]
69. Rodríguez-Cuevas, A.; Peña, E.R.; Rodríguez-Cobo, L.; Lomer, M.; López-Higuera, J.M. Low-cost fiber specklegram sensor for noncontact continuous patient monitoring. *J. Biomed. Opt.* **2017**, *22*, 037001. [CrossRef] [PubMed]
70. Dhall, A.; Chhabra, J.; Aulakh, N. Intrusion detection system based on speckle pattern analysis. *Exp. Tech.* **2005**, *29*, 25–31. [CrossRef]
71. Kotov, O.I.; Kosareva, L.I.; Liokumovich, L.B.; Markov, S.I.; Medvedev, A.V.; Nikolaev, V.M. Multichannel signal detection in a multimode optical-fiber interferometer: Reducing the effect of spurious signals. *Tech. Phys. Lett.* **2000**, *26*, 991–995. [CrossRef]
72. Szustakowski, M.; Ciurapiński, W.; Życzkowski, M.; Wróbel, J.; Dulski, R.; Markowskia, P. Security–orientated Plastic Optical Fiber sensor in Modalmetric Configuration. *Procedia Eng.* **2012**, *47*, 916–923. [CrossRef]
73. Rodriguez-Cobo, L.; Lomer, M.; Lopez-Higuera, J.-M. Fiber Specklegram-Multiplexed Sensor. *J. Light. Technol.* **2015**, *33*, 2591–2597. [CrossRef]
74. Pan, K.; Uang, C.-M.; Cheng, F.; Yu, F.T.S. Multimode fiber sensing by using mean-absolute speckle-intensity variation. *Appl. Opt.* **1994**, *33*, 2095–2098. [CrossRef] [PubMed]
75. Lujo, I.; Klokoc, P.; Komljenovic, T.; Sipus, Z. Measuring structural vibrations with a multimode fiber optical sensor. In Proceedings of the 2007 19th International Conference on Applied Electromagnetics and Communications (ICECom), Dubrovnik, Croatia, 24–26 September 2007; pp. 1–4. [CrossRef]
76. Fujiwara, E.; Ri, Y.; Wu, Y.T.; Fujimoto, H.; Suzuki, C.K. Evaluation of image matching techniques for optical fiber specklegram sensor analysis. *Appl. Opt.* **2018**, *57*, 9845–9854. [CrossRef] [PubMed]
77. Yu, F.T.S.; Zhang, J.; Pan, K.; Zhao, D.; Ruffin, P.B. Fiber vibration sensor that uses the speckle contrast ratio. *Opt. Eng.* **1995**, *34*, 236–239. [CrossRef]
78. Kulchin, Y.N.; Vitrik, O.B.; Lantsov, A.D. Correlation method for processing speckles of signals from single-fibre multimode interferometers by using charge-coupled devices. *Quantum Electron.* **2006**, *36*, 339–342. [CrossRef]
79. Yu, F.T.S.; Wen, M.; Yin, S.; Uang, C.-M. Submicrometer displacement sensing using inner-product multimode fiber speckle fields. *Appl. Opt.* **1993**, *32*, 4685–4689. [CrossRef]
80. Kulchin, Y.N.; Vitrik, O.B.; Lantsov, A.D. Correlation processing of signals of a single-fibre multimode interferometer upon excitation of few modes during measurements of deformation effects. *Quantum Electron.* **2008**, *38*, 56–58. [CrossRef]

81. Fujiwara, E.; dos Santos, M.F.M.; Suzuki, C.K. Optical fiber specklegram sensor analysis by speckle pattern division. *Appl. Opt.* **2017**, *56*, 1585–1590. [CrossRef]
82. Rodriguez-Cobo, L.; Lomer, M.; Cobo, A.; Lopez-Higuera, J.M. Optical fiber strain sensor with extended dynamic range based on specklegrams. *Sens. Actuators A Phys.* **2013**, *203*, 341–345. [CrossRef]
83. Kulchin, Y.N.; Obukh, V.F. Spatial filtering of radiation from a multimode waveguide in determination of hydroacoustic pressures. *Sov. J. Quantum Electron.* **1986**, *16*, 424–426. [CrossRef]
84. A Bykovskiĭ, Y.; Vitrik, O.B.; Kulchin, Y.N. Amplitude spatial filtering in the processing of signals from a single-fiber multimode interferometer. *Sov. J. Quantum Electron.* **1990**, *20*, 1288–1290. [CrossRef]
85. Kamshilin, A.A.; Jaaskelainen, T.; Kulchin, Y.N. Adaptive correlation filter for stabilization of interference-fiber-optic sensors. *Appl. Phys. Lett.* **1998**, *73*, 705–707. [CrossRef]
86. Potton, R.J. Adaptive spatial filtering using photochromic glass. *Meas. Sci. Technol.* **1999**, *10*, 1315–1318. [CrossRef]
87. Newaz, A.; Faruque, O.; Al Mahmud, R.; Sagor, R.H.; Khan, M.Z.M. Machine-Learning-Enabled Multimode Fiber Specklegram Sensors: A Review. *IEEE Sens. J.* **2023**, *23*, 20937–20950. [CrossRef]
88. Liu, Y.; Li, G.; Qin, Q.; Tan, Z.; Wang, M.; Yan, F. Bending recognition based on the analysis of fiber specklegrams using deep learning. *Opt. Laser Technol.* **2020**, *131*, 106424. [CrossRef]
89. Li, G.; Liu, Y.; Qin, Q.; Zou, X.; Wang, M.; Ren, W. Feature Extraction Enabled Deep Learning From Specklegram for Optical Fiber Curvature Sensing. *IEEE Sens. J.* **2022**, *22*, 15974–15984. [CrossRef]
90. Lu, S.; Tan, Z.; Li, G.; Jingya, Y. A Sensitized Plastic Fiber Sensor for Multi-Point Bending Measurement Based on Deep Learning. *IEEE Photonics J.* **2021**, *13*, 8600107. [CrossRef]
91. Ding, Z.; Zhang, Z. 2D tactile sensor based on multimode interference and deep learning. *Opt. Laser Technol.* **2020**, *136*, 106760. [CrossRef]
92. Pal, D.; Agadarov, S.; Beiderman, Y.; Beiderman, Y.; Kumar, A.; Zalevsky, Z. Non-invasive blood glucose sensing by machine learning of optic fiber-based speckle pattern variation. *J. Biomed. Opt.* **2022**, *27*, 097001. [CrossRef]
93. Chen, P.; You, C.; Ding, P. Event classification using improved salp swarm algorithm based probabilistic neural network in fiber-optic perimeter intrusion detection system. *Opt. Fiber Technol.* **2020**, *56*, 102182. [CrossRef]
94. Cuevas, A.R.; Fontana, M.; Rodriguez-Cobo, L.; Lomer, M.; Lopez-Higuera, J.M. Machine Learning for Turning Optical Fiber Specklegram Sensor into a Spatially-Resolved Sensing System. Proof of Concept. *J. Light. Technol.* **2018**, *36*, 3733–3738. [CrossRef]
95. Gao, H.; Hu, H. Spatially-resolved bending recognition based on a learning-empowered fiber specklegram sensor. *Opt. Express* **2023**, *31*, 7671–7683. [CrossRef] [PubMed]
96. Wei, M.; Tang, G.; Liu, J.; Zhu, L.; Liu, J.; Huang, C.; Zhang, J.; Shen, L.; Yu, S. Neural Network Based Perturbation-Location Fiber Specklegram Sensing System Towards Applications With Limited Number of Training Samples. *J. Light. Technol.* **2021**, *39*, 6315–6326. [CrossRef]
97. Markvart, A.A.; Liokumovich, L.B.; Ushakov, N.A. Simultaneous measurement of strain and bend with a fiber optic SMS structure. In Proceedings of the Optical Fiber Sensors Conference 2020 Special Edition, Washington, DC, USA, 8–12 June 2020; p. W4.57. [CrossRef]
98. Markvart, A.A.; Liokumovich, L.B.; Ushakov, N.A. Fiber Optic SMS Sensor for Simultaneous Measurement of Strain and Curvature. *Tech. Phys. Lett.* **2022**, *48*, 34. [CrossRef]
99. Galarza, M.; Perez-Herrera, R.A.; Leandro, D.; Judez, A.; López-Amo, M. Spatial-frequency multiplexing of high-sensitivity liquid level sensors based on multimode interference micro-fibers. *Sens. Actuators A Phys.* **2020**, *307*, 111985. [CrossRef]
100. Rota-Rodrigo, S.; Lopez-Aldaba, A.; Perez-Herrera, R.A.; Bautista, M.d.C.L.; Esteban, O.; Lopez-Amo, M. Simultaneous Measurement of Humidity and Vibration Based on a Microwire Sensor System Using Fast Fourier Transform Technique. *J. Light. Technol.* **2016**, *34*, 4525–4530. [CrossRef]
101. Cardona-Maya, Y.; Del Villar, I.; Socorro, A.B.; Corres, J.M.; Matias, I.R.; Botero-Cadavid, J.F. Wavelength and Phase Detection Based SMS Fiber Sensors Optimized With Etching and Nanodeposition. *J. Light. Technol.* **2017**, *35*, 3743–3749. [CrossRef]
102. Petrov, A.; Kotov, O.; Golovchenko, A. Measurement of External Impact by an Intermodal Fiber Interferometer with Spectral Interrogation and Fourier Transform of Output Signals. In Proceedings of the 2023 International Conference on Electrical Engineering and Photonics (EExPolytech), St. Petersbourg, Russia, 20–21 October 2023; pp. 406–409. [CrossRef]
103. Theodosiou, A. Adaptive Refractive Index Measurements via Polymer Optical Fiber Speckle Pattern Analysis. *IEEE Sens. J.* **2024**, *24*, 287–291. [CrossRef]
104. Leung, C.-Y.; Chang, I.-F.; Hsu, S. Fiberoptic Line-Sensing System for Perimeter Protection Against Intrusion. In *Optical Fiber Sensors*; Optica Publishing Group: Tokyo, Japan, 1986; p. 54. [CrossRef]
105. Leng, J.; Asundi, A. NDE of smart structures using multimode fiber optic vibration sensor. *NDT E Int.* **2002**, *35*, 45–51. [CrossRef]
106. Wang, J.-J.; Yan, S.-C.; Xu, F. Speckle-based fiber sensor for temperature measurement. In Proceedings of the 2017 16th International Conference on Optical Communications and Networks (ICOCN), Wuzhen, China, 7–10 August 2017; pp. 1–3. [CrossRef]
107. Wang, J.-J.; Yan, S.-C.; Ruan, Y.-P.; Xu, F.; Lu, Y.-Q. Fiber-Optic Point-Based Sensor Using Specklegram Measurement. *Sensors* **2017**, *17*, 2429. [CrossRef] [PubMed]
108. Musin, F.; Mégret, P.; Wuilpart, M. Fiber-Optic Surface Temperature Sensor Based on Modal Interference. *Sensors* **2016**, *16*, 1189. [CrossRef] [PubMed]

109. Regez, B.; Sayeh, M.; Mahajan, A.; Figueroa, F. A novel fiber optics based method to measure very low strains in large scale infrastructures. *Measurement* **2009**, *42*, 183–188. [CrossRef]
110. Fujiwara, E.; da Silva, L.E.; Marques, T.H.R.; Cordeiro, C.M.B. Polymer optical fiber specklegram strain sensor with extended dynamic range. *Opt. Eng.* **2018**, *57*, 116107. [CrossRef]
111. Fujiwara, E.; Wu, Y.T.; dos Santos, M.F.M.; Schenkel, E.A.; Suzuki, C.K. Development of a tactile sensor based on optical fiber specklegram analysis and sensor data fusion technique. *Sens. Actuators A Phys.* **2017**, *263*, 677–686. [CrossRef]
112. Garcia-Valenzuela, A.; Tabib-Azar, M. Fiber-optic force and displacement sensor based on speckle detection with 0.1 nN and 0.1 Å resolution. *Sens. Actuators A Phys.* **1993**, *36*, 199–208. [CrossRef]
113. Wang, X.; Song, L.; Wang, X.; Lu, S.; Li, J.; Zhang, P.; Fang, F. An Ultrasensitive Fiber-End Tactile Sensor With Large Sensing Angle Based on Specklegram Analysis. *IEEE Sens. J.* **2023**, *23*, 30394–30402. [CrossRef]
114. Kinet, D.; Wuilpart, M.; Reginster, M.; Caucheteur, C.; Musin, F. Cost-effective optical fiber gas leakage detector around buried pipelines. In *Optical Sensing and Detection V*; SPIE Photonics Europe: Strasbourg, France, 2018; p. 1068018. [CrossRef]
115. Ramprasad, B.; Bai, T.R. Speckle-based fibre-optic current sensor. *Opt. Laser Technol.* **1984**, *16*, 156–159. [CrossRef]
116. Wang, B.; Fu, J.Y.; Liu, Y.; Guo, R.; Yu, F.T.S. Displacement Sensing with Hetero-Core Fiber Specklegram. In Proceedings of the Optical Science and Technology, the SPIE 49th Annual Meeting, Denver, CO, USA, 2–6 August 2004; p. 164. [CrossRef]
117. Liu, Y.; Qin, Q.; Liu, H.-H.; Tan, Z.-W.; Wang, M.-G. Investigation of an image processing method of step-index multimode fiber specklegram and its application on lateral displacement sensing. *Opt. Fiber Technol.* **2018**, *46*, 48–53. [CrossRef]
118. Chen, W.; Feng, F.; Chen, D.; Lin, W.; Chen, S.-C. Precision non-contact displacement sensor based on the near-field characteristics of fiber specklegrams. *Sens. Actuators A Phys.* **2019**, *296*, 1–6. [CrossRef]
119. Osório, J.H.; Cabral, T.D.; Fujiwara, E.; Franco, M.A.; Amrani, F.; Delahaye, F.; Gérôme, F.; Benabid, F.; Cordeiro, C.M. Displacement sensor based on a large-core hollow fiber and specklegram analysis. *Opt. Fiber Technol.* **2023**, *78*, 103335. [CrossRef]
120. Wang, X.; Yang, Y.; Li, S.; Wang, X.; Zhang, P.; Lu, S.; Yu, D.; Zheng, Y.; Song, L.; Fang, F. A reflective multimode fiber vector bending sensor based on specklegram. *Opt. Laser Technol.* **2024**, *170*, 110235. [CrossRef]
121. Warren-Smith, S.C.; Kilpatrick, A.D.; Wisal, K.; Nguyen, L.V. Multimode optical fiber specklegram smart bed sensor array. *J. Biomed. Opt.* **2022**, *27*, 067002. [CrossRef] [PubMed]
122. Bennett, A.; Beiderman, Y.; Agdarov, S.; Beiderman, Y.; Hendel, R.; Straussman, B.; Zalevsky, Z. Monitoring of vital bio-signs by analysis of speckle patterns in a fabric-integrated multimode optical fiber sensor. *Opt. Express* **2020**, *28*, 20830–20844. [CrossRef] [PubMed]
123. Markvart, A.; Kulik, D.; Petrov, A.; Liokumovich, L.; Ushakov, N. Pulse Wave Measurement Using Fiber-Optic Intermodal Interferometric Sensor. In *International Youth Conference on Electronics, Telecommunications and Information Technologies: Proceedings of the YETI 2021, St. Petersburg, Russia*; Springer: Berlin/Heidelberg, Germany, 2022; pp. 429–436.
124. Pang, Y.-N.; Liu, B.; Liu, J.; Wan, S.-P.; Wu, T.; Yuan, J.; Xin, X.; He, X.-D.; Wu, Q. Singlemode-Multimode-Singlemode Optical Fiber Sensor for Accurate Blood Pressure Monitoring. *J. Light. Technol.* **2022**, *40*, 4443–4450. [CrossRef]
125. Zhao, F.; Lin, W.; Guo, P.; Hu, J.; Liu, S.; Yu, F.; Zuo, G.; Wang, G.; Liu, H.; Chen, J.; et al. Demodulation of DBR Fiber Laser Sensors With Speckle Patterns. *IEEE Sens. J.* **2023**, *23*, 26022–26030. [CrossRef]
126. Lin, W.; Liu, B.; Liu, H.; Yang, C.; Zhang, H. Fibre-optic salinity sensor based on multimode fibre specklegram analysis. *Meas. Sci. Technol.* **2021**, *32*, 115110. [CrossRef]
127. Fujiwara, E.; da Silva, L.E.; Cabral, T.D.; de Freitas, H.E.; Wu, Y.T.; Cordeiro, C.M.d.B. Optical Fiber Specklegram Chemical Sensor Based on a Concatenated Multimode Fiber Structure. *J. Light. Technol.* **2019**, *37*, 5041–5047. [CrossRef]
128. Mu, G.; Liu, Y.; Qin, Q.; Tan, Z.; Li, G.; Wang, M.; Yan, F. Refractive Index Sensing Based on the Analysis of D-Shaped Multimode Fiber Specklegrams. *IEEE Photonics Technol. Lett.* **2020**, *32*, 485–488. [CrossRef]
129. Arı, F.; Şerbetçi, H.; Navruz, I. Tapered fiber optic refractive index sensor using speckle pattern imaging. *Opt. Fiber Technol.* **2023**, *79*, 103366. [CrossRef]
130. Al Zain, M.; Karimi-Alavijeh, H.; Moallem, P.; Khorsandi, A.; Ahmadi, K. A High-Sensitive Fiber Specklegram Refractive Index Sensor With Microfiber Adjustable Sensing Area. *IEEE Sens. J.* **2023**, *23*, 15570–15577. [CrossRef]
131. Cai, L.; Wang, M.; Zhao, Y. Investigation on refractive index sensing characteristics based on multimode fiber specklegram. *Meas. Sci. Technol.* **2023**, *34*, 015125. [CrossRef]
132. Guo, P.; Peng, X.; Li, J.; Zhou, Z.; Hu, J.; Xue, C.; Hu, J.; Li, J.; Dang, H.; Chen, J.; et al. Refractive Index Detection of Liquid Analyte in Broad Range Using Multimode Fiber Speckle Sensor. In Proceedings of the 2022 Asia Communications and Photonics Conference (ACP), Shenzhen, China, 5–8 November 2022; pp. 1981–1983. [CrossRef]
133. Liu, Y.; Lin, W.; Zhao, F.; Liu, Y.; Sun, J.; Hu, J.; Li, J.; Chen, J.; Zhang, X.; Vai, M.I.; et al. A Multimode Microfiber Specklegram Biosensor for Measurement of CEACAM5 through AI Diagnosis. *Biosensors* **2024**, *14*, 57. [CrossRef] [PubMed]
134. Feng, F.; Chen, W.; Chen, D.; Lin, W.; Chen, S.-C. In-situ ultrasensitive label-free DNA hybridization detection using optical fiber specklegram. *Sens. Actuators B Chem.* **2018**, *272*, 160–165. [CrossRef]
135. Inalegwu, O.C.; Ii, R.E.G.; Huang, J. A Machine Learning Specklegram Wavemeter (MaSWave) Based on a Short Section of Multimode Fiber as the Dispersive Element. *Sensors* **2023**, *23*, 4574. [CrossRef]
136. Tan, H.; Li, B.; Crozier, K.B. Optical fiber speckle spectrometer based on reversed-lens smartphone microscope. *Sci. Rep.* **2023**, *13*, 12958. [CrossRef] [PubMed]
137. Redding, B.; Alam, M.; Seifert, M.; Cao, H. High-resolution and broadband all-fiber spectrometers. *Optica* **2014**, *1*, 175. [CrossRef]

138. Jamali, R.; Nazari, F.; Ghaffari, A.; Velu, S.K.P.; Moradi, A.-R. Speckle tweezers for manipulation of high and low refractive index micro-particles and nano-particle loaded vesicles. *Nanophotonics* **2021**, *10*, 2915–2928. [CrossRef]
139. Volpe, G.; Kurz, L.; Callegari, A.; Volpe, G.; Gigan, S. Speckle optical tweezers: Micromanipulation with random light fields. *Opt. Express* **2014**, *22*, 18159–18167. [CrossRef]
140. Moslehi, B.; Goodman, J.W.; Rawson, E.G. Bandwidth estimation for multimode optical fibers using the frequency correlation function of speckle patterns. *Appl. Opt.* **1983**, *22*, 995–999. [CrossRef]
141. Ahn, T.-J.; Moon, S.; Kim, S.; Oh, K.; Kim, D.Y.; Kobelke, J.; Schuster, K.; Kirchhof, J. Frequency-domain intermodal interferometer for the bandwidth measurement of a multimode fiber. *Appl. Opt.* **2006**, *45*, 8238–8243. [CrossRef] [PubMed]
142. Feng, Z.; Sakr, H.; Hayes, J.R.; Fokoua, E.R.N.; Ding, M.; Poletti, F.; Richardson, D.J.; Slavík, R. Hollow-core fiber with stable propagation delay between −150 °C and +60 °C. *Opt. Lett.* **2023**, *48*, 763–766. [CrossRef] [PubMed]
143. Kumar, S.H.; Kumar, C.J.; Somnath, B.; Kumar, G.P. Multi-Fiber Optic 2d-Array Device for Sensing and Localizing Environment Perturbation Using Speckle Image Processing. US6590194B2, 27 March 2001.
144. Thompson, D.; Joshua, G.; Keenan, R. Fiber-Optic Mat Sensor. US7532781B2, 19/772007, 12 May 2009.
145. Kotov, O.I.; Chapalo, I.E.; Medvedev, A.V. Dependence of the signal of a multimode fiber-optic interferometer on the mode power distribution. *Tech. Phys. Lett.* **2014**, *40*, 509–512. [CrossRef]
146. Kotov, O.I.; Chapalo, I.E. External impact localization in a distributed intermodal fiber interferometer. *Tech. Phys. Lett.* **2015**, *41*, 1139–1142. [CrossRef]
147. Kotov, O.; Chapalo, I. *Mode-Mode Fiber Interferometer with Impact Localization Ability*; SPIE Photonics Europe: Brussels, Belgium, 2016; p. 98992J. [CrossRef]
148. Chapalo, I.; Kotov, O.; Petrov, A. Dual-wavelength one-directional multimode fiber interferometer with impact localization ability. In *Optical Sensing and Detection V*; SPIE Photonics Europe: Strassburg, France, 2018; p. 106801V. [CrossRef]
149. Chapalo, I.; Theodosiou, A.; Kalli, K.; Kotov, O. Multimode fiber interferometer with embedded long period grating. In *Seventh European Workshop on Optical Fibre Sensors; In Proceedings of the Seventh European Workshop on Optical Fibre Sensors*; Limassol, Cyprus, 1–4 October 2019, p. 111990Q. [CrossRef]
150. Chapalo, I.; Chah, K.; Gusarov, A.; Ioannou, A.; Pospori, A.; Nan, Y.-G.; Kalli, K.; Mégret, P. Gamma-radiation enhancement of sensing properties of FBGs in a few-mode polymer CYTOP fiber. *Opt. Lett.* **2023**, *48*, 1248–1251. [CrossRef]